

## Ensemble Kalman, adaptive Gaussian mixture, and particle flow filters for optimized earthquake occurrence estimation

Diab-Montero, Hamed Ali; Stordal, Andreas S.; van Leeuwen, Peter Jan; Vossepoel, Femke C.

**DOI**

[10.1016/j.cageo.2024.105836](https://doi.org/10.1016/j.cageo.2024.105836)

**Publication date**

2025

**Document Version**

Final published version

**Published in**

Computers and Geosciences

**Citation (APA)**

Diab-Montero, H. A., Stordal, A. S., van Leeuwen, P. J., & Vossepoel, F. C. (2025). Ensemble Kalman, adaptive Gaussian mixture, and particle flow filters for optimized earthquake occurrence estimation. *Computers and Geosciences*, 196, Article 105836. <https://doi.org/10.1016/j.cageo.2024.105836>

**Important note**

To cite this publication, please use the final published version (if applicable). Please check the document version above.

**Copyright**

Other than for strictly personal use, it is not permitted to download, forward or distribute the text or part of it, without the consent of the author(s) and/or copyright holder(s), unless the work is under an open content license such as Creative Commons.

**Takedown policy**

Please contact us and provide details if you believe this document breaches copyrights. We will remove access to the work immediately and investigate your claim.



## Research paper

# Ensemble Kalman, adaptive Gaussian mixture, and particle flow filters for optimized earthquake occurrence estimation

Hamed Ali Diab-Montero <sup>a</sup><sup>\*</sup>, Andreas S. Stordal <sup>b,c</sup>, Peter Jan van Leeuwen <sup>d,e</sup>,  
Femke C. Vossepoel <sup>a</sup>

<sup>a</sup> Delft University of Technology, Department of Geoscience and Engineering, The Netherlands

<sup>b</sup> NORCE, Norwegian Research Center, Nygårdssporten 112, 5008 Bergen, Norway

<sup>c</sup> Department of Mathematics, University of Bergen, Postboks 7803, 5020 Bergen, Norway

<sup>d</sup> Department of Atmospheric Science, Colorado State University, Fort Collins, CO, USA

<sup>e</sup> Department of Meteorology, University of Reading, Reading, UK



## ARTICLE INFO

Dataset link: <http://doi.org/10.4121/f0f075f2-f45c-4f8c-9d1d-bde03baeae33>

## Keywords:

Data assimilation

Inverse theory

Uncertainty quantification

Probabilistic forecasting

Earthquake dynamics

Seismic cycle

## ABSTRACT

Probabilistic forecasts are regarded as the highest achievable goal when predicting earthquakes, but limited information on stress, strength, and governing parameters of the seismogenic sources affects their accuracy. Ensemble data-assimilation methods, such as the Ensemble Kalman Filter (EnKF), estimate these variables by combining physics-based models and observations. While the EnKF has demonstrated potential in perfect model experiments using earthquake simulators governed by rate-and-state friction (RSF) laws, challenges arise from the non-Gaussian distribution of state variables during seismic cycle transitions. This study investigates the Adaptive Gaussian Mixture Filter (AGMF) and the Particle Flow Filter (PFF) as alternatives for improved stress and velocity estimation in earthquake sequences compared to Gaussian-based methods like the EnKF. We test the AGMF and the PFF's performance using Lorenz 96 and Burridge–Knopoff 1D models which are, respectively, standard simplified atmospheric and earthquake models. This approach, using widely recognized and commonly used testbed models in their fields, makes the methods and findings accessible to both the data assimilation and seismology communities, while supporting comparisons and collaboration. We test these models in periodic, and aperiodic conditions, and analyze the impact of assuming Gaussian priors on the estimates of the ensemble methods. The PFF demonstrated comparable performance in chaotic scenarios, yielding lower RMSE for the estimates of the Lorenz 96 models and stronger resilience to underdispersion for the Burridge–Knopoff 1D models. This is vital given the limited and sparse historical earthquake data, underscoring the PFF's potential in enhancing earthquake forecasting. These results emphasize the need for careful data assimilation method selection in seismological modeling.

## 1. Introduction

Data assimilation (DA) techniques are used for forecasting geophysical systems with uncertain conditions, by combining information from physics-based simulations and observational data to estimate states or parameters (Evensen et al., 2022; Bannister, 2017; van Leeuwen, 2010; Evensen, 2003). DA's utility spans from weather forecasting (Evensen, 1994; Reichle, 2008) to hydrologic models (Liu et al., 2012) and oil production (Aanonsen et al., 2009; Evensen and Eikrem, 2018). Geophysical systems, characterized by their sensitivity to initial conditions and potential for significant error growth over time, underscore the importance of DA's trajectory correction (Carrasi et al., 2022). The Adaptive Gaussian Mixture Filter (AGMF) (Stordal et al., 2011)

and Particle Flow Filter (PFF) (Hu and van Leeuwen, 2021) are non-Gaussian ensemble DA methods, suited for chaotic systems which are characterized by being sensitive to the initial conditions and show aperiodic behavior. The AGMF bridges particle filter's importance sampling weights via Gaussian mixtures with the Ensemble Kalman Filter's update, while PFF solves a transport differential equation to iteratively transform the prior distribution to the posterior. The effectiveness of these methods has been tested in atmospheric physics models noticing more accurate estimates (Stordal et al., 2011; Hu and van Leeuwen, 2021; Hu et al., 2024), especially when dealing with non-Gaussian distributions and non-linear observation operators. Similarly, when estimating earthquake and fault slip occurrences challenges arise from

\* Corresponding author.

E-mail address: [h.a.diabmontero@tudelft.nl](mailto:h.a.diabmontero@tudelft.nl) (H.A. Diab-Montero).

the non-Gaussian distribution of state variables during seismic cycle transitions (Diab-Montero et al., 2023).

In the realm of earthquake forecasting, the *rate-and-state friction* (RSF) law marks a significant advancement over traditional slip-weakening friction models. Developed from laboratory experiments on slip instabilities and rate weakening (Marone, 1998), the primary advantage of the RSF law is its versatility in describing a broad spectrum of laboratory data (Ruina, 1983; Dieterich, 1979). This versatility enables it to more accurately model the initiation, progression, and termination of seismic events, offering a comprehensive understanding of earthquake dynamics that previous models could not adequately capture. However, the inherent non-linearity of the RSF law leads to stiff differential equations in numerical simulations (Erickson et al., 2008), which pose challenges when solving these equations. This often requires techniques such as adaptive time stepping or may lead to the creation of non-Gaussian distributions when using an ensemble of simulations (Diab-Montero et al., 2023), especially when parameters are uncertain. While regularization of the RSF law improves numerical stability and does not necessarily produce periodic earthquake sequences, it can, in some cases, still result in simpler, more periodic solutions that may not fully capture the complex recurrence of earthquake events in nature (Lapusta and Rice, 2003; Erickson et al., 2008, 2011). This limitation underscores the need for sophisticated data assimilation methods that can handle such complexity and uncertainty, such as accounting for model error—representing unknown or unmodeled physical processes and inaccuracies in the model physics—by augmenting the state vector with additional terms, an approach we use in our work.

Over the past decade, various data assimilation methods have been developed to address different components of the earthquake process, including estimation of seismic wavefield, calculation of slip rates, and forecasting of fault slip events (Maeda et al., 2015; Oba et al., 2020). These methods, although tested through perfect-model experiments (Kano et al., 2013; Hori et al., 2014), face challenges in modeling RSF, leading to non-Gaussian distributions (van Dinther et al., 2019; Hirahara and Nishikiori, 2019). Ensemble distributions of slow acceleration models are primarily Gaussian, which facilitate the use of Ensemble Kalman filters which have proven useful to correct the state of the earthquake models and an effective manner to influence the evolution of the system (van Dinther et al., 2019; Diab-Montero et al., 2023). However, non-Gaussian distributions are typical in fast acceleration models which pose challenges for the EnKF (Banerjee et al., 2023; Diab-Montero et al., 2023). Thus, it is essential to develop data assimilation methods that can manage non-Gaussian distributions for estimating earthquake occurrences.

In this study, we evaluate the advantages of using the AGMF and the PFF for non-Gaussian data assimilation of earthquake occurrences in systems dominated by RSF. These methods have previously been compared in simplistic atmospheric models, such as the Lorenz 96 system, and here we extend this analysis to investigate which findings and lessons from those comparisons are transferable to earthquake dynamics. Given the differing physics of these systems, we aim to test these methods in controlled and explainable conditions tailored to earthquake modeling. We assess how the estimates of these filters of the shear stress, velocity, and the state  $\theta$  of the RSF law compare to those from the EnKF under periodic and chaotic conditions. Moreover, we explore the use of including a model error term for estimating non-periodic sequences in the presence of parameter bias. By understanding the implications of these different methods and assumptions, we aim to contribute to more accurate and efficient earthquake forecasting methodologies.

The outline of the paper is as follows: Section 2 explains the workings of the ensemble-based data assimilation methods (EnKF, AGMF, and PFF) and introduces the perfect-model experiments conducted on Lorenz 96 and Burridge–Knopoff earthquake models under periodic and chaotic conditions. Section 3 compares the estimates provided by the three methods for different observation coverages, and the evolution of

the ensemble spread for each method across the seismic cycle. Besides, in this section we present some results when including model error as part of the state vector for dealing with parameter bias. Section 4 discusses the influence of prior information on the analysis update of the PFF. The final section presents conclusions about the filter performance for earthquake occurrence estimation under periodic and chaotic conditions.

## 2. Methodology

### 2.1. Data assimilation

Data assimilation helps to better estimate the evolution of a system by knowledge of its dynamics with observations thereof. The variables of interest are represented as,

$$\mathbf{z}^T = \left( \mathbf{z}_\psi^T, \mathbf{z}_\alpha^T \right), \quad (1)$$

where  $\mathbf{z}$  is the *state vector*, and the components  $\mathbf{z}_\psi$  and  $\mathbf{z}_\alpha$  signify system states and parameters, respectively. In this study, we only include the states ( $\mathbf{z}_\psi$ ) in the state vector.

The estimation process entails two steps. The first, the *forecast step*, that evolves the variables from a previous time  $t - 1$  to a future time  $t$  using the system's dynamics:

$$\mathbf{z}_t = \mathcal{M}_{t:t-1}(\mathbf{z}_{t-1}) + \mathbf{q}_t, \quad (2)$$

with  $\mathcal{M}_{t:t-1}$  as the forward model operator and  $\mathbf{q}_t$  as the model error.

The second, the *analysis step*, where we update our knowledge of the system, is based on Bayes' theorem:

$$p(\mathbf{z}|\mathbf{d}) = \frac{p(\mathbf{d}|\mathbf{z})p(\mathbf{z})}{p(\mathbf{d})}, \quad (3)$$

where  $p(\mathbf{z})$ , the prior, is derived from the state values obtained from the forecast step,  $p(\mathbf{d}|\mathbf{z})$  is the likelihood of the observations, and  $p(\mathbf{d})$  is the evidence.

Observations are represented by:

$$\mathbf{d}_t = \mathcal{H}_t(\mathbf{z}_t) + \epsilon_t, \quad (4)$$

where  $\mathbf{d}_t$  is the observation vector,  $\mathcal{H}_t$  is the observation operator that maps the state vector to observation space, and  $\epsilon_t$  denotes measurement errors. The observation operator can be non-linear, but in this work we assumed it is linear.

### The Ensemble Kalman Filter

We use in this study the stochastic Ensemble Kalman Filter (EnKF) (Evensen, 2003), an ensemble-based data assimilation method and a Monte Carlo approach for approximating the Bayesian update outlined in Eq. (3). The EnKF combines the forward numerical model's information (prior) with its deviation from observations (likelihood) to yield a posterior state vector estimate. We assume Gaussian distributions for the prior, and the likelihood probability density functions (pdfs). Our state vector ensemble is represented as:

$$\mathbf{z}_n^T = \left( \mathbf{z}_\psi^T, \mathbf{z}_\alpha^T \right)_n, \quad 1 \leq n \leq N_m, \quad (5)$$

where  $n$  signifies an ensemble member, with the ensemble containing  $N_m$  realizations. The prior is given by  $\mathbf{z}_n^f \sim \mathcal{N}(\overline{\mathbf{z}}_n^f, \mathbf{C}_{zz}^f)$ , with the forecast superscript ( $f$ ) signifying prior data from the forward numerical model. The overline denote the ensemble average. The covariance, which describe the uncertainties of states, is approximated as:

$$\mathbf{C}_{zz}^f = \frac{1}{N-1} \left( \mathbf{z}^f - \overline{\mathbf{z}}^f \right) \left( \mathbf{z}^f - \overline{\mathbf{z}}^f \right)^T. \quad (6)$$

Localization on the prior covariance matrix is applied via a Schur product:

$$\mathbf{C}_{zz,loc}^f \leftarrow \rho_{i,j} \circ \mathbf{C}_{zz}^f, \quad (7)$$

where,

$$\rho_{i,j} = \exp\left\{-\left(\frac{i-j}{r_{in}}\right)^2\right\}, \quad (8)$$

and  $i, j = 1, \dots, N_c$ .  $N_c$  is the number of cells of the model, and  $r_{in}$  is the decorrelation radius which is dependent on the type of model used. For a detailed explanation of localization, please refer to [Appendix A](#). Additionally, inflation is applied to the analysis covariance matrix using:

$$\mathbf{C}_{zz,infl}^a \leftarrow \rho_{infl} \mathbf{C}_{zz}^a, \quad (9)$$

with  $\rho_{infl}$ , the inflation factor, slightly greater than one.

We adopt a perturbed-observations scheme, assuming observational errors to be Gaussian ( $\epsilon_n \sim \mathcal{N}(0, C_{dd})$ ) and observation errors to be uncorrelated. The perturbed observation vector is:

$$\mathbf{d}_n = \mathbf{d} + \epsilon_n, \quad 1 \leq n \leq N_m, \quad (10)$$

and the covariance error matrix is:

$$\mathbf{C}_{dd} = \frac{1}{N-1} \sum_{n=1}^N \epsilon_n \epsilon_n^T. \quad (11)$$

The EnKF combines the prior, observation vector, and their covariances to compute the posterior distribution using:

$$\mathbf{z}_n^a = \mathbf{z}_n^f + \mathbf{K} [\mathbf{d}_n - \mathbf{H}\mathbf{z}_n^f], \quad 1 \leq n \leq N_m, \quad (12)$$

where  $\mathbf{K}$  is the Kalman gain matrix and  $\mathbf{H}$  is the observation operator that we assume is linear. The Kalman gain is:

$$\mathbf{K} = \mathbf{C}_{zz}^f \mathbf{H}^T (\mathbf{H} \mathbf{C}_{zz}^f \mathbf{H}^T + \mathbf{C}_{dd})^{-1}, \quad (13)$$

and determines how much we adjust our estimate of the system's state by balancing the new observations information against the prior forecast, based on their uncertainties. A higher gain gives more weight to the observations, while a lower gain favors the forecast. For more details, refer to [Evensen \(2003\)](#), [Evensen et al. \(2022\)](#).

## 2.2. Methods with non-Gaussian prior assumptions

### Adaptive Gaussian Mixture Filter

The Adaptive Gaussian Mixture Filter (AGMF) serves as a bridging formulation between ensemble Kalman filters and particle filters analysis updates ([Stordal et al., 2011](#); [Van Leeuwen et al., 2019](#); [Stordal and Lorentzen, 2014](#)). This transition capability stems from a two-stage update process in the analysis step.

**1. Ensemble Member Update:** The ensemble members and their covariance matrix undergo an update, based on Eq. (12) but with a dampened background covariance matrix:

$$\mathbf{z}_n^a = \mathbf{z}_n^f + h^2 \mathbf{C}_{zz}^f \mathbf{H}^T (h^2 \mathbf{H} \mathbf{C}_{zz}^f \mathbf{H}^T + \mathbf{C}_{dd})^{-1} [\mathbf{d}_n - \mathbf{H}\mathbf{z}_n^f], \quad 1 \leq n \leq N_m, \quad (14)$$

where  $h$  is the bandwidth parameter with  $h \in [0, 1]$ . The update is the same as the EnKF for  $h = 1$  and no update at  $h = 0$ .

**2. Importance Sampling:** Ensemble members are assigned weights following a Gaussian mixture:

$$w_i^n = \mathcal{N}(\mathbf{d}_n - \mathbf{H}\mathbf{z}_i^f, h^2 \mathbf{H} \mathbf{C}_{zz}^f \mathbf{H}^T + \mathbf{C}_{dd}) w_{i-1}^n. \quad (15)$$

The weight normalization ensures their collective sum equals one:

$$\bar{w}_i^n = \frac{w_i^n}{\sum_n w_i^n}. \quad (16)$$

A bridging parameter  $\beta_t$  is introduced to avoid weight collapse. It adaptively minimizes weights towards uniform ones:

$$w_i^n = \beta_t \bar{w}_i^n + (1 - \beta_t) N_m^{-1}, \quad (17)$$

by modulating both  $\beta_t$  and  $h$ , a smooth transition between behaving like an ensemble Kalman filter, which is efficient for Gaussian assumptions, and a more flexible filter that can handle non-Gaussian distributions. The optimal value for  $\beta_t$  is defined as:

$$\beta_t = \frac{N_{eff}}{N_m} = \frac{1}{N_m \sum_{n=1}^{N_m} (\bar{w}_i^n)^2}. \quad (18)$$

Finally, we use the resampling method used in [Stordal et al. \(2011\)](#) to further avoid ensemble degeneracy when the effective sample size  $N_{eff}$  is less than 80% of the ensemble size  $N_m$ .

### Particle Flow Filter

The particle flow filter is a method that iteratively transforms equally weighted samples from a prior distribution to the posterior distribution ([Hu and van Leeuwen, 2021](#)), in contrast to the conventional particle filter that assigns different weights to its samples based on their likelihood given the observations and relies on these weights to approximate the posterior distribution. The transformation follows the solution of a differential equation of the type:

$$\frac{d}{ds} \mathbf{z}_s = \mathbf{f}_s(\mathbf{z}_s), \quad (19)$$

where  $\mathbf{z}_s$  transitions from the prior to the posterior over an artificial pseudo time  $s \in [0, \infty]$ :

$$q_0(\mathbf{z}) = p(\mathbf{z}), \quad (20)$$

$$q_\infty(\mathbf{z}) = p(\mathbf{z}|\mathbf{d}),$$

The particle flow,  $\mathbf{f}_s$ , can be determined either through the likelihood-factorization approach or by minimizing a distance measure between the intermediate pdf  $q_s$  and  $q_\infty$  ([Evensen et al., 2022](#)). This study uses the latter method where the Kullback–Leibler (KL) divergence serves as the distance measure:

$$KL(q_s) = \int q_s(\mathbf{z}) \log\left(\frac{q_s(\mathbf{z})}{q_\infty(\mathbf{z})}\right) d\mathbf{z}. \quad (21)$$

The particle flow exists in a reproducing kernel Hilbert space (RKHS) with a kernel  $\mathbf{K}_{ker}$ , and it is designed to always reduce the KL divergence over pseudo time:

$$\mathbf{f}_s = \mathbf{C}_{zz}^f \int q_s(\mathbf{z}) \{\mathbf{K}_{ker}(\mathbf{z}, \cdot) \nabla_{\mathbf{z}} \log(p(\mathbf{z}|\mathbf{d})) + \nabla_{\mathbf{z}} \cdot \mathbf{K}_{ker}(\mathbf{z}, \cdot)\}. \quad (22)$$

With a particle representation for  $q_s$ , the flow becomes:

$$\mathbf{f}_s(\mathbf{z}) = \frac{1}{N_m} \mathbf{C}_{zz}^f \sum_{n=1}^{N_m} \{\mathbf{K}_{ker}(\mathbf{z}_s^n, \mathbf{z}) \nabla_{\mathbf{z}_s^n} \log(p(\mathbf{z}_s^n|\mathbf{d})) + \nabla_{\mathbf{z}_s^n} \cdot \mathbf{K}_{ker}(\mathbf{z}_s^n, \mathbf{z})\}. \quad (23)$$

which follows the form of a Fokker–Planck equation ([Evensen et al., 2022](#)) with an attracting term and a repelling term respectively on the right hand side. After discretizing the equation in pseudo time, the state vector's evolution is described as:

$$\mathbf{z}_{s+\Delta s} = \mathbf{z}_s + \frac{\Delta s}{N_m} \mathbf{C}_{zz}^f \sum_{n=1}^{N_m} \{\mathbf{K}_{ker}(\mathbf{z}_s^n, \mathbf{z}_s) \nabla_{\mathbf{z}_s^n} \log(p(\mathbf{z}_s^n|\mathbf{d})) + \nabla_{\mathbf{z}_s^n} \cdot \mathbf{K}_{ker}(\mathbf{z}_s^n, \mathbf{z}_s)\}. \quad (24)$$

The kernel  $\mathbf{K}_{ker}(\mathbf{z}_s^n, \mathbf{z})$  measures how each of the ensemble members contribute to the local particle flow:

$$\mathbf{K}_{ker}(\mathbf{z}_s^n, \mathbf{z}) = \exp\left(-\frac{1}{2} \frac{(z_{s,(j)}^n - z_{s,(j)})^2}{\alpha \sigma_{(j)}^2}\right), \quad (25)$$

where  $z_{s,(j)}$  is the  $j$ th component of the  $\mathbf{z}_s$  vector,  $\alpha$  is the multiplication factor determining the width of the kernel, and  $\sigma_{(j)}$  is the standard deviation of the  $j$ th component of the state vector. In the case of an infinite number of particles, the solution of the PFF is independent of the kernel's choice ([Lu et al., 2019](#)). In this study, a matrix-valued Gaussian kernel is used as in [Hu and van Leeuwen \(2021\)](#). Unlike a scalar kernel that applies a single distance measure uniformly across all components of the state vector, the matrix-valued kernel allows

for independent distance measurements in each of the states of the particles. The attracting term can be expressed using Bayes theorem:

$$\nabla_{\mathbf{z}} \log p(\mathbf{z}|\mathbf{d}) = \nabla_{\mathbf{z}} \log p(\mathbf{z}) + \nabla_{\mathbf{z}} \log p(\mathbf{d}|\mathbf{z}). \quad (26)$$

For Gaussian distributions, gradients for the likelihood and the prior are given by:

$$\nabla_{\mathbf{z}} \log p(\mathbf{d}|\mathbf{z}) = \mathbf{H}^T \mathbf{C}_{\text{dd}}^{-1} (\mathbf{d} - \mathbf{H}\mathbf{z}), \quad (27)$$

and

$$\nabla_{\mathbf{z}} \log p(\mathbf{z}) = -\mathbf{C}_{zz}^f^{-1} (\mathbf{z} - \bar{\mathbf{z}}_b), \quad (28)$$

where  $\bar{\mathbf{z}}_b$  is the prior mean.

For a more comprehensive explanation of these methods and their theoretical foundations, readers are encouraged to refer to [Evensen et al. \(2022\)](#).

## 2.3. Forward modeling

### 2.3.1. Lorenz 96 model

The Lorenz 96 model is a simplified yet effective representation of the chaotic behavior of atmospheric dynamics ([Lorenz and Emanuel, 1998](#)) commonly used as benchmark in testing data assimilation techniques. The equation that models Lorenz 96 is:

$$\frac{dx_i}{dt} = (x_{i+1} - x_{i-1})x_{i-1} - x_i + F \quad (29)$$

with boundary conditions  $x_{-1} = x_{N_c-1}$ ,  $x_0 = x_{N_c}$ ,  $x_{N_c+1} = x_1$  and constraint  $N_c \geq 4$ . Here,  $x_i$  represents a state element, for instance, temperature, at a sector along a latitude circle divided into  $N_c$  equal sectors ([van Kekem, 2018](#)). The equation features advection, damping, and forcing effects. The system exhibits coherent structures and even chaotic behavior based on parameters  $F$  and  $N_c$ .

### 2.3.2. The 1D discrete Burridge–Knopoff model

Similar to the Lorenz 96 model, the Burridge–Knopoff (BK) model is a simplified benchmark, but in this case of earthquake sequences. It is characterized by a spring-block slider system ([Burridge and Knopoff, 1967](#)). In our study, the 1-D BK model comprises multiple blocks connected by elastic springs with stiffness  $k_\mu$ , depicted in [Fig. 1](#). The multiple-block structure in the 1-D BK model approximates the spatial distribution of stress along a fault. Each block interacts with its neighbors, simulating how stress builds up, transfers, and propagates, capturing key features of fault dynamics like stress heterogeneity and slip. These blocks are elastically coupled (with stiffness  $k_\lambda$ ) to a rigid plate moving at speed  $v_p$  across a frictionally rough surface, serving as an analogue for a 1-D earthquake fault ([Carlson et al., 1991](#)). This research adopts the 1-D BK system modeling methodology of [Erickson et al. \(2011\)](#). The system of ordinary differential equations (ODEs) used is:

$$\begin{aligned} \dot{u}_i &= \bar{v}_i, \\ \dot{v}_i &= \gamma_\mu^2 (\bar{u}_{i-1} - 2\bar{u}_i + \bar{u}_{i+1}) - \gamma_\lambda^2 \bar{u}_i - \frac{\gamma_\mu^2}{\xi} \bar{\tau}_i, \\ \dot{\bar{\Theta}}_i &= -(\bar{v}_i + 1) (\bar{\Theta}_i + (1 + \epsilon) \log(\bar{v}_i + 1)). \end{aligned} \quad (30)$$

Several modifications and simplifications were applied to achieve this non-dimensional system of ODEs, including adopting the non-dimensional variables from [Madariaga \(1998\)](#), [Erickson et al. \(2011\)](#). In these equations,  $\bar{u}$  represents the non-dimensional slip of the blocks,  $\bar{v}$  is the non-dimensional slip rate and  $\bar{\Theta}$  is the non-dimensional state of the RSF law, not to be confused with the *statevector*  $\mathbf{z}$ . We also have the following parameters:  $\gamma_\mu$  and  $\gamma_\lambda$  that are non-dimensional frequencies,  $\bar{f}$  which is the scaled steady-state friction coefficient,  $\xi$  that is the non-dimensional spring constant, and  $\epsilon$  which measures the sensitivity of the velocity relaxation. Studies have shown that the 1-D BK models can exhibit periodic, chaotic behaviors and other

**Table 1**

Non-dimensional rate-and-state friction parameters for the 1-D Burridge–Knopoff model coupled with rate-and-state friction.

Parameter	Symbol	Periodic	Chaotic
Sensitivity of the velocity relaxation	$\epsilon$	0.3	0.5
Non-dimensional spring constant	$\xi$	0.5	0.5
Non-dimensional frequency	$\gamma_\mu$	0.5	0.5
Non-dimensional frequency	$\gamma_\lambda$	$\sqrt{0.2}$	$\sqrt{0.2}$
Scaled steady-state friction coefficient	$\bar{f}$	3.2	3.2

complex dynamical phenomena depending on the choice of these parameters ([Erickson et al., 2008, 2011](#)). Additionally,  $\bar{\tau}$  is the shear stress that is governed by the rate-and-state friction law ([Ruina, 1983](#)) which is employed to explain the friction on the rough surface:

$$\bar{\tau}_i = \bar{f} + \bar{\Theta}_i + \log(\bar{v}_i + 1), \quad (31)$$

where we see the relation of the shear stress with the *rate* ( $\bar{v}$ ), and the *state* ( $\bar{\Theta}$ ) that fluctuate depending on interseismic (stick) and coseismic (slip) phases. Given the choice of non-dimensional parameters, like  $\epsilon$  and  $\xi$ , can produce smooth transitions from the interseismic to the coseismic phase resembling a behavior more similar to Slow Slip Events (SSES) ([Diab-Montero et al., 2023](#)) rather than earthquakes, while a different choice can also produce sharper transitions ([Banerjee et al., 2023; Diab-Montero et al., 2023](#)) typical of earthquakes with fast slip-rates. This versatility makes the Burridge–Knopoff model a good test-bed model for our data assimilation experiments.

In the Burridge–Knopoff model coupled with rate-and-state friction, we frequently encounter the logarithmic term  $\log(\bar{v})$ . As explained in multiple works, such as [Erickson et al. \(2008\)](#), [Noda et al. \(2009\)](#), [Rojas et al. \(2009\)](#), as  $\bar{v} \rightarrow 0$ , this term becomes exponentially negative. This behavior is also reflected in the local Jacobian ([Erickson et al., 2008](#)), where the eigenvalues in the Jacobian become exceptionally large. Using the modified term  $\log(\bar{v}+1)$ , as we do in this work, partially alleviates this issue.

Typically, negative eigenvalues relate to stability, as they imply decaying dynamics. However, the rapid decay of  $\bar{v}$  leads to numerical stiffness in the system, which requires very small time steps with standard numerical methods to achieve stable solutions. Even with implicit methods, the time step size remains constrained by accuracy requirements ([Erickson et al., 2008, 2011](#))—if the time step is too large, the logarithmic term becomes undefined. To address this, we employed an embedded fourth-order explicit Runge–Kutta method with a small step size for solving the ODEs.

## 2.4. Perfect model experiments

In our study, we used perfect model experiments to evaluate the performance of the data assimilation methods. In these experiments, we generated a synthetic true solution and synthetic observations, and evaluated how well the filters estimated the state variables. We specifically used Lorenz 96 models of 20 cells and 1D Burridge–Knopoff models of 20 blocks. For both we used ensembles of 100 members. For the Lorenz 96, the state vector consists on the values of  $x$  for each cell. For the 1-D Burridge–Knopoff models the state vector is,

$$\mathbf{z}_n^T = (\bar{\tau}^T, \bar{\mathbf{u}}^T, \log(\bar{\mathbf{v}} + 1)^T, \bar{\Theta}^T)_n, \quad 1 \leq n \leq N_m, \quad (32)$$

where we employ  $\log(\bar{\mathbf{v}} + 1)$  instead of  $\bar{\mathbf{v}}$  to impose a positivity constrain (see [Fig. 2](#)).

We utilized a fourth-order Runge–Kutta (RK4) scheme with a  $\Delta t = 0.01$  time step to generate a reference solution, for each type of model. For the Lorenz 96 models, we used  $F = 1.2$  for the periodic case and  $F = 8.0$  for the chaotic case. For the BK model we used the frictional parameters from [Table 1](#).

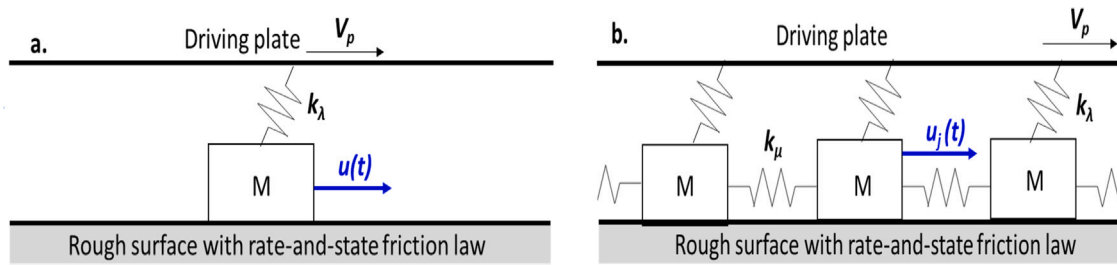


Fig. 1. Schematic representation of the Burridge Knopoff models coupled with the rate-and-state friction law (a) single degree of freedom slider block coupled by a spring loader plate representing the other side of the fault. (b) spring connected chain of blocks, elastically coupled to a driver plate moving at a constant velocity  $V_p$ . The surface upon which the blocks slip is rough and the friction force holding the slider in place is governed by a rate-state friction law.

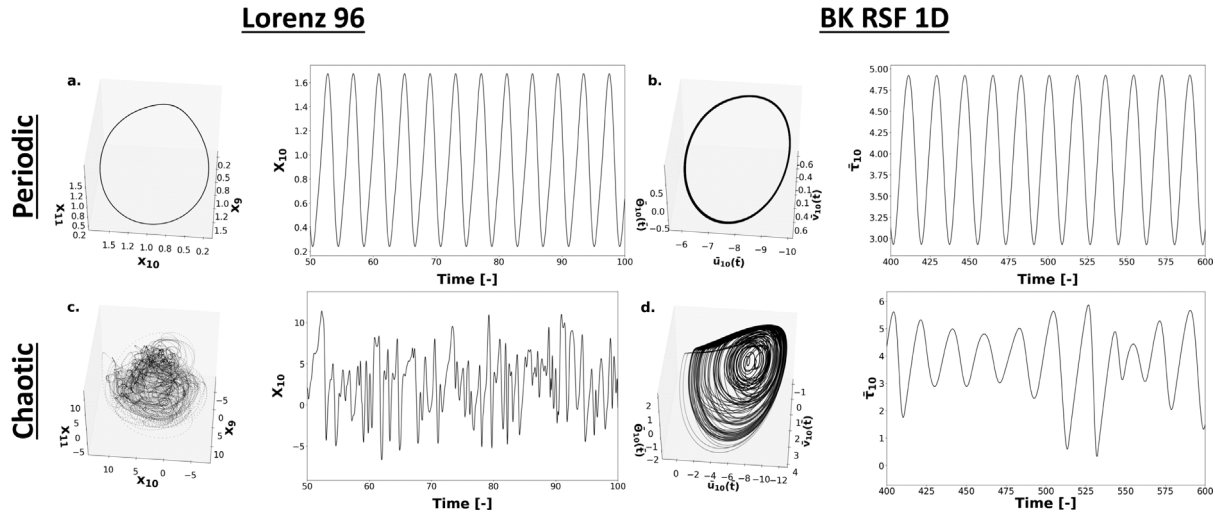


Fig. 2. Schematic representation of the evolution of the Lorenz 96 (a, c) and 1-D Burridge–Knopoff model coupled with rate-and-state friction (b, d) use for creating the synthetic truth of the perfect model experiments. Phase diagrams of the Lorenz 96 models under (a) periodic ( $F = 1.2$ ) and (c) chaotic ( $F = 8.0$ ) conditions, and the evolution of the state of the 10th cell through time for the periodic and chaotic case respectively. Phase diagrams of the BK-RSF 1D model under (b) periodic and (d) chaotic conditions, and the evolution of the shear stress for the 10th block through time for the periodic and chaotic case respectively.

Our examination considered synthetic observations using different spatial observation densities with coverages of 100% and 50%. For the Lorenz 96, we assimilate observations of the state  $x$ . For the 1-D Burridge–Knopoff model, the observation vector is:

$$d^T = (\bar{\tau}^T, \log(\bar{v} + 1)^T). \quad (33)$$

We assumed Gaussian uncorrelated observation errors with diagonal matrices  $C_{dd}$ . We defined the uncertainties ( $\sigma_\epsilon$ ) using typical observation uncertainties used in other works for the Lorenz 96 model (Stordal et al., 2011), and for the 1-D Burridge–Knopoff model, (Banerjee et al., 2023). Specifically, synthetic observational noise was modeled as  $\sigma_\epsilon^2 \sim \mathcal{N}(0, \sigma_\epsilon^2)$ , where the errors are sampled from a normal distribution with zero mean and variance  $\sigma_\epsilon^2$ . For the variable  $x$  of Lorenz 96 we use a standard deviation of 1 for the observation error. For  $\bar{\tau}$  and  $\log(\bar{v} + 1)$  of the seismological models we used a standard deviation of 0.6. We extract synthetic observations by perturbing the true data values using these uncertainties and use the same synthetic observations for the perfect model experiments conducted with the different data assimilation methods.

Using the periodic solutions we define the cycle duration. The Lorenz 96’s periodic cycle covers 4 time units (equivalent to 400 steps). Based on this, we used a default rate of 8 observations per cycle or which is the same 0.5 time units (50 timesteps) between observations for the synthetic experiments. For the BK-RSF 1D, its cycle spans approximately 18 time units (or 1800 steps). We used then a default rate of 8 observations per cycle or which is the same 2.25 time units (225 timesteps) between observations.

For the localization of the prior covariance matrices, and defining the best hyperparameters for each filter, we followed the steps shown in Appendix A.

### 3. Results

In this section, we present the outcomes from perfect model experiments, focusing on comparing the three data assimilation methods: EnKF, AGMF, and PFF. Our aim is to evaluate these methods in terms of accuracy, using RMSE (Root Mean Square Error) values, which is defined as

$$RMSE \ X(t) = \sqrt{\frac{1}{N_c} \sum_{j=1}^{N_c} (\bar{x}_j(t) - x_{j,truth}(t))^2}, \quad (34)$$

where  $\bar{x}_j$  is the ensemble mean for the  $j$ th component of the state vector and the  $x_{j,truth}$  is the  $j$ th component of the truth. We also use the ensemble spread (the range or variability of estimates from an ensemble), assessed through rank histograms (Anderson, 1996; Hamill, 2001), which are commonly use graphical tools used to evaluate the reliability, and spread of ensemble forecasts. This comparison extends across different phases of the seismic cycle for the 1-D BK models, emphasizing how the ensemble spread changes with each phase of the seismic cycle.

#### 3.1. Lorenz 96

Fig. 3 depicts the RMSE outcomes for the variable  $x_i$  over time. Notably, RMSE values for the periodic Lorenz 96 model are consistently

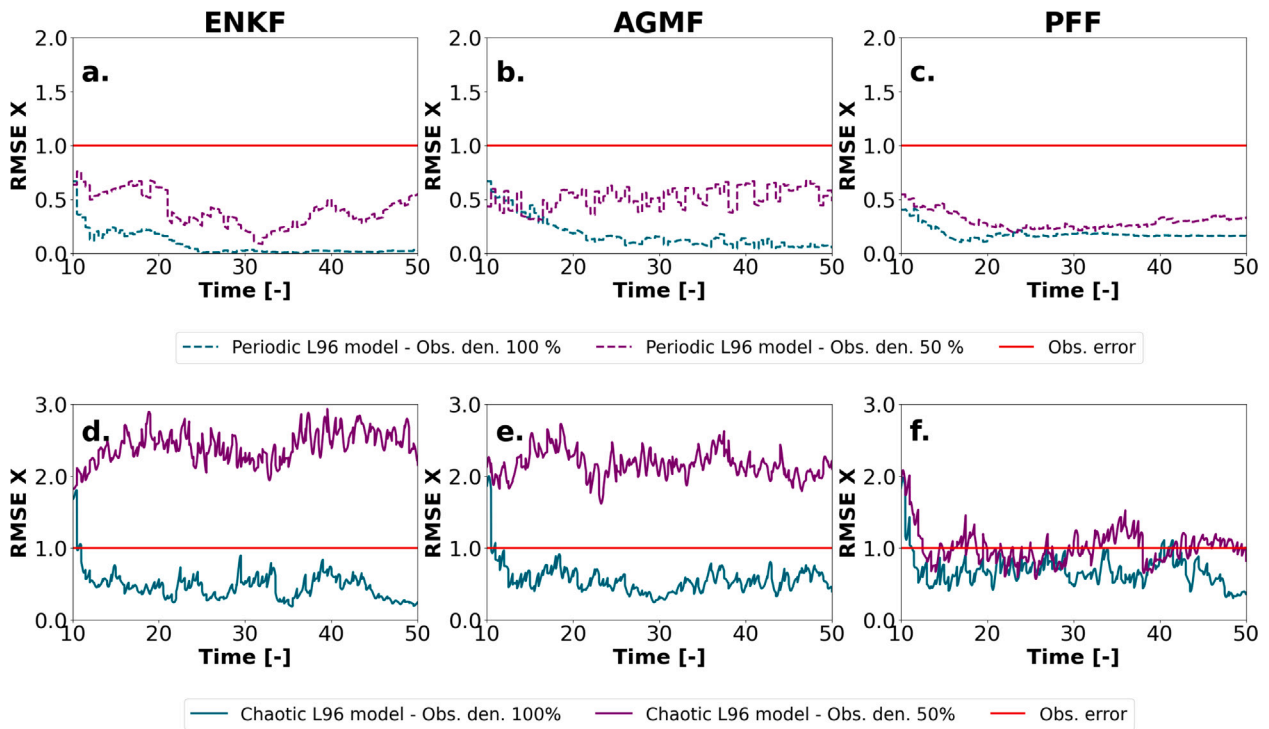


Fig. 3. Comparison of RMSEs for different observation densities for the Lorenz 96 between EnKF (a, d), AGMF (b, e), PFF (c, f).

lower than for its chaotic counterpart. In the chaotic case, all three filters yield RMSE values below the observation error when using an observation density of 100% (i.e., full cell coverage, where observations are available for all grid cells). In comparison, only the PFF achieves values below the observation error with 50% coverage. In contrast, the EnKF shows the highest RMSE at 50% coverage. The AGMF also shows higher RMSE values than the observation error, which are slightly lower than the EnKF's RMSE values. These findings align with the observations by Hu and van Leeuwen (2021) on the 40 variable-Lorenz 96 model, which noticed similar contrasts between the Local Ensemble Transform Kalman Filter (LETKF) and PFF. The increased non-linearity in variable relationships during chaotic periods underscores the necessity for a non-Gaussian, non-linear filter, especially when full variable coverage is unavailable. Alternatively, it is possible to introduce iterations on the AGMF and EnKF schemes (e.g., an MDA-type update) to achieve lower RMSE values.

### 3.2. Burridge Knopff 1D model

#### 3.2.1. Analysis of errors and underdispersion

Fig. 4 shows the RMSEs of the EnKF, the AGMF, and the PFF for the slip-rate  $\bar{v}_i$ , which is an observed variable. The results show the comparison of the RMSEs when observing all the blocks (left column) and when only observing half of them (right column) for the periodic and the chaotic case. The results show that the three methods have estimates with errors lower than the observation error, as expected. The EnKF shows the lowest errors when having access to the observations of all the blocks. Interestingly, the AGMF has lower errors than the EnKF when fewer observations are available. The case with fewer observations presents a more challenging condition for the estimation, which makes the importance sampling step of the AGMF useful to capture the distributions of the variables better. The RMSE results show the same trend for the estimates of the shear stress  $\bar{\tau}$ .

Fig. 5 show the RMSEs of the EnKF, the AGMF and the PFF for the state  $\bar{\theta}$  which is not observed also called a hidden state. The results

show that for all methods the error decreases as more observation are assimilated with time. For the periodic case the ENKF and the AGMF have the lowest errors. However, for the chaotic case the differences between the RMSE values for the different methods are less noticeable.

We find that the ensemble spread greatly decreases after these first assimilation windows. This indicates a problem of underdispersion, also called overconfidence. A possible remedy to this problem is the use of covariance inflation. However, even when testing with high inflation factors, the issue of underdispersion on the rank histograms persisted. Interestingly, as we will see, the Particle Flow Filter does not experience this sudden decrease in the ensemble spread.

The rank-histograms (Fig. 6) highlight that the filters have problems of underdispersion. The resampling step of the AGMF can help to keep a wider ensemble, especially in the periodic case, but this resampling seems insufficient for reducing the underdispersion in the spread. Further refinement of the PFF's hyperparameters, such as bandwidth and learning rate, could yield more accurate and precise results while preserving an ensemble spread wide enough to correspond to the posterior uncertainties.

Fig. 7 shows a comparison of the time series estimates of the slip-rate ( $\bar{v}$ ) for the EnKF, AGMF, and PFF ensemble members for a periodic sequence while Fig. 8 does it for a chaotic sequence. The histograms of the ensemble distribution of the different methods show that the PFF maintains a broad posterior distribution in both cases. In contrast, the AGMF and the EnKF have very narrow ensemble distributions. Despite these narrow distributions, both methods have estimates that are very close to the truth. However, a consequence of the very narrow distributions is that the EnKF and AGMF ensemble will not cover the true state in certain phases.

#### 3.2.2. Sensitivity on model error

Recent findings, e.g. Gualandi et al. (2023), show how having a deterministic model representing a laboratory setup of a direct shear type of machine, a setup with a material sample between two plates where one plate is moved horizontally while the other remains fixed,

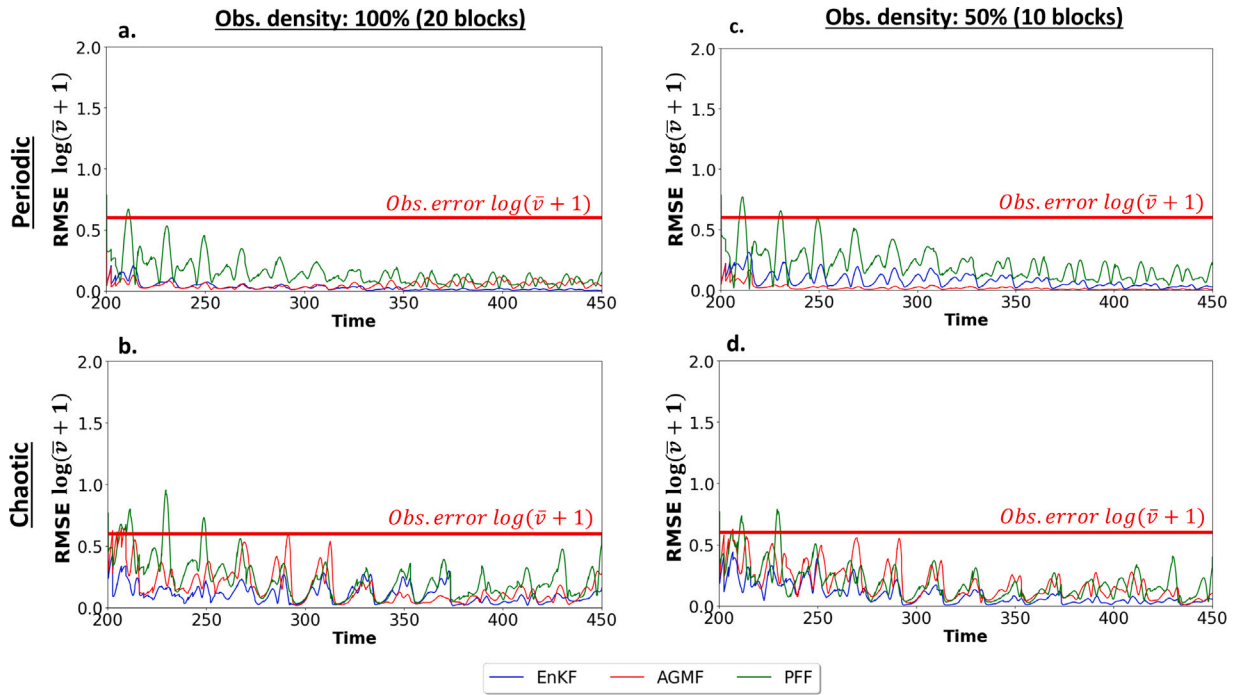


Fig. 4. Comparison of the RMSEs for the estimates of the logarithm of the velocity ( $\log(\bar{v} + 1)$ ) of the EnKF (blue), the AGMF (red) and the PFF (green) for the 1-D Burridge Knopoff model coupled with rate-and-state friction. The upper row shows the comparison for the periodic case (a, c), and the lower row for the chaotic case (b, d). The results correspond to an observation density of 100% of the blocks for the left column (a, b) and 50% of the blocks in the right column (c, d).

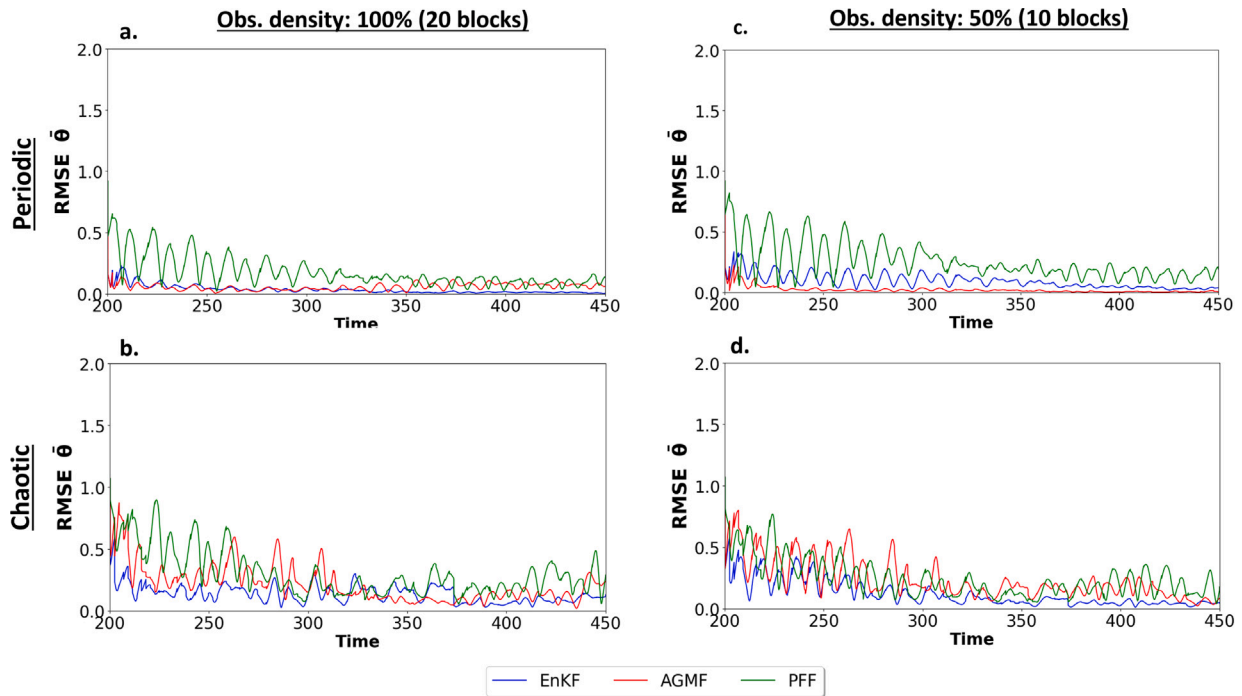


Fig. 5. Comparison of the RMSEs for the estimates of the state  $\bar{\theta}$  of the EnKF (blue), the AGMF (red) and the PFF (green) for the 1-D Burridge Knopoff model coupled with rate-and-state friction. The upper row shows the comparison for the periodic case (a, c), and the lower row for the chaotic case (b, d). The results correspond to an observation density of 100% of the blocks for the left column (a, b) and 50% of the blocks in the right column (c, d).

can constrain the solutions to just a set of possible states of the system. Gualandi et al. (2023) showed that even for a laboratory experiment with controlled conditions, introducing stochastic terms in the system of ordinary differential equations was the most accurate approach for explaining the system’s behavior.

We can achieve a similar result of this stochastic term by including model error terms in the state vector of the data assimilation. These

model errors can account for missing physics or errors in the dynamical forward model. In this context, introducing a model error can improve the estimation of the system’s dynamics and help maintain ensemble spread. This is especially useful for addressing underdispersion that can occur when the regularized rate-and-state friction (RSF) formulation, which is intended to improve numerical stability, occasionally leads

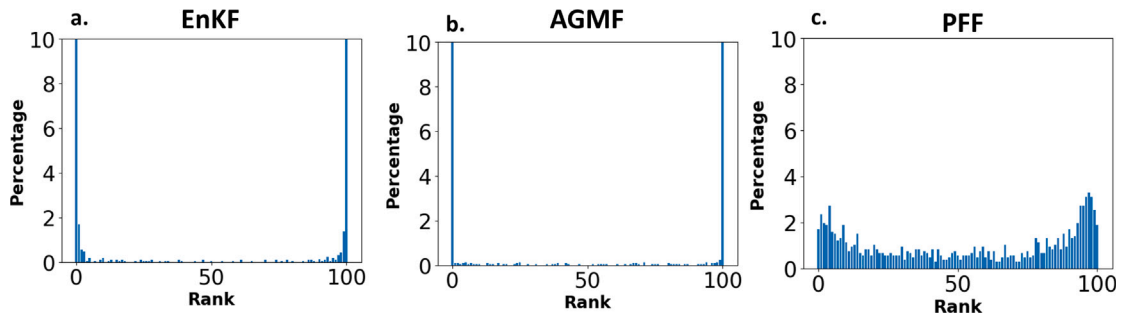


Fig. 6. Rank histogram for the estimates of the (a) EnKF, (b) AGMF, and the (c) PFF for the periodic case.

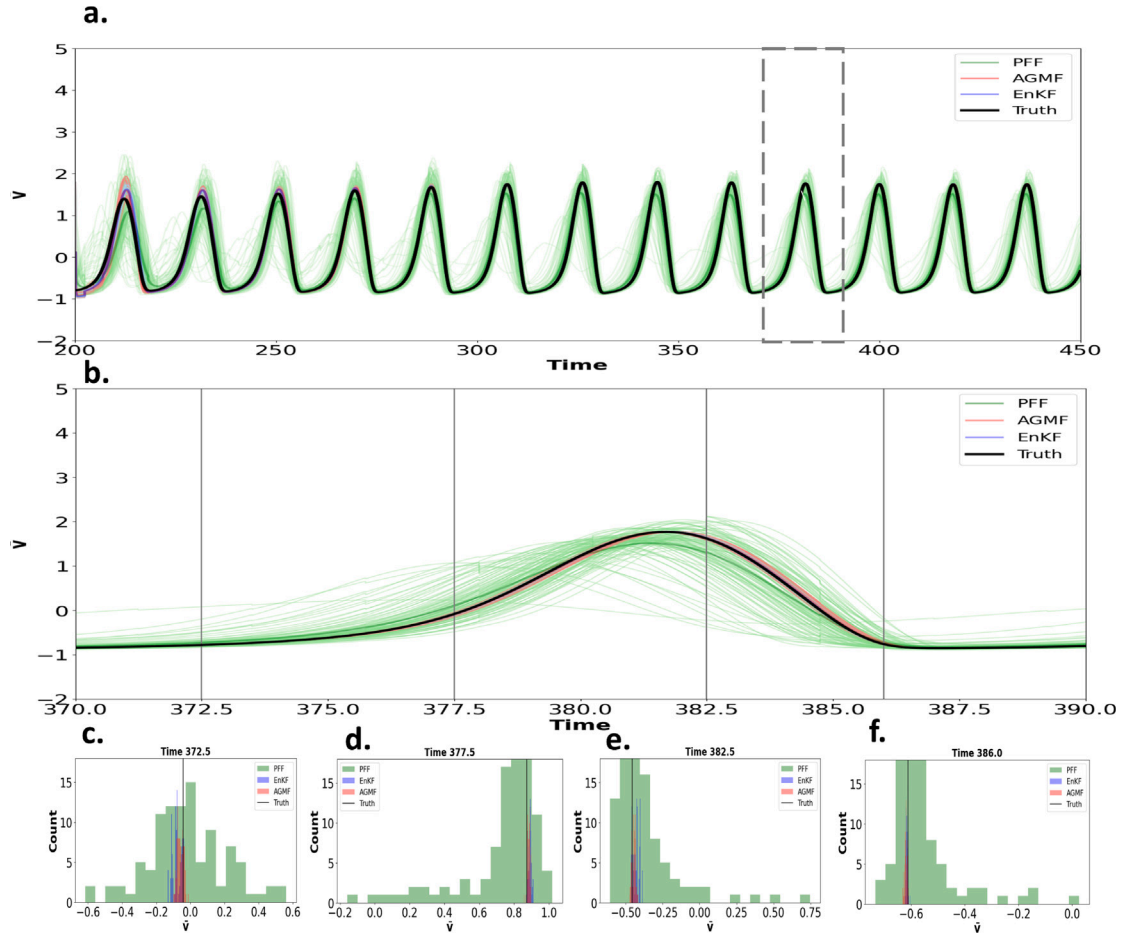


Fig. 7. Comparison of the estimates of the slip-rate ( $\bar{v}$ ) of block 10 for the EnKF (blue), the AGMF (red), and the PFF (green) for estimating an earthquake occurrence for a periodic event. The true time series of the slip-rate is shown with a solid black line. We compare the ensemble distribution for the interseismic phase (c, d) during the coseismic phase (e), and at the end of the coseismic phase (f).

to more periodic or simplified solutions in methods like the Ensemble Kalman Filter (EnKF).

To evaluate the effect of introducing a stochastic term in the equations, we visualize the effect of using such a term in a forward simulation of the 1-D Burridge Knopoff model. We aim to verify that we can use values of  $\epsilon$  that produce periodic solutions and still estimate aperiodic behavior. The advantage of maintaining  $\epsilon$  fixed is that we avoid further instability issues or changes in the frictional behavior of the system. For this, we perturbed the shear stress  $\bar{\tau}$  as follows:

$$\bar{\tau}_i = \bar{f} + \bar{\Theta}_i + \log(\bar{v}_i + 1) + q, \quad (35)$$

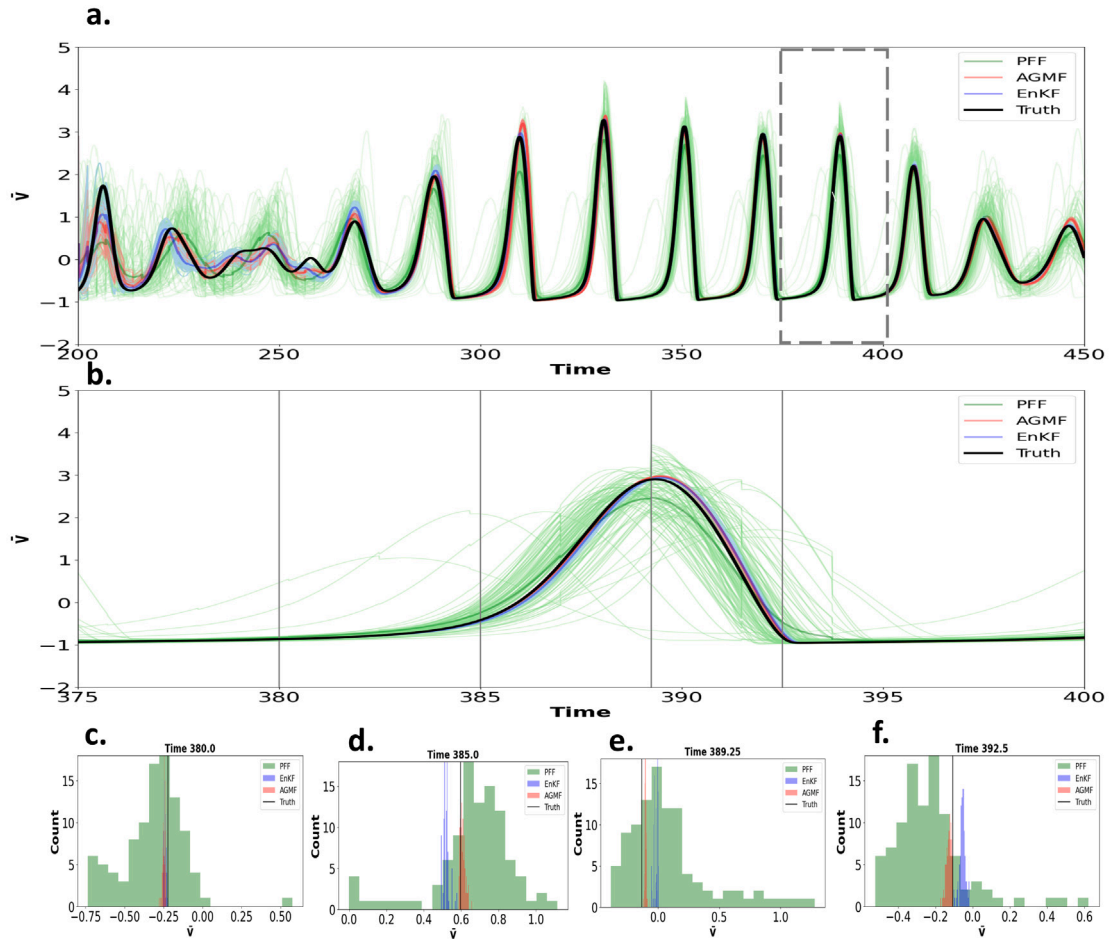
where  $q$  is the stochastic term that follows a distribution  $q \sim \mathcal{N}(0, C_{qq})$ . We assume that the covariance matrix  $C_{qq}$  is diagonal with  $\sigma_q \in [0, 1]$ .

Fig. 9 shows the evolution of the phase diagram of block 10 of a 1-D Burridge Knopoff with  $\epsilon = 0.3$  in the periodic regime when increasing  $\sigma_q$ . We can see how the phase diagrams become more and more similar to the chaotic case shown in Fig. 1d, with an  $\epsilon = 0.5$ .

We propose to make the model error a function of the slip-rate as follows:

$$q = f(\bar{v}) = q_{error}\bar{v}. \quad (36)$$

This model error term  $q$  can be explained as a radiation damping term that compensates for the loss of energy caused by the seismic waves after the fault's slip, and which is commonly included in quasi-dynamic models (Crupi and Bizzarri, 2013). The term  $q_{error}$  is interpreted when using radiation damping as a ratio between the elastic



**Fig. 8.** Comparison of the estimates of the slip-rate ( $\bar{v}$ ) of block 10 for the EnKF (blue), the AGMF (red), and the PFF (green) for estimating an earthquake occurrence for a chaotic event. The true time series of the slip-rate is shown with a solid black line. We compare the ensemble distribution for the interseismic phase (c,d) during the coseismic phase (e), and at the end of the coseismic phase (f).

medium rigidity and the S-wave velocity away from the fault plane. Here, we expand the state vector to include the  $q_{error}$  and treat it as an additional parameter,

$$\mathbf{z}_n^T = (\bar{\tau}^T, \bar{\mathbf{u}}^T, \log(\bar{v} + 1)^T, \bar{\Theta}^T, \mathbf{q}_{error}^T)_n, \quad 1 \leq n \leq N_m. \quad (37)$$

The advantage of reformulating the assimilation this way, which is more similar to a parameter estimation exercise, is that knowing  $q_{error}$  also helps us to investigate which processes could be missing/wrongly represented in the forward model, and use it to improve this model for forecasting applications. Fig. 10a shows the slip-rate estimates of an EnKF with periodic ensemble members that assimilate synthetic observations obtained from a chaotic truth without including the model error in the state vector, while Fig. 10b shows the estimates when it is included. For the ensemble  $\epsilon_n \sim \mathcal{N}(0.3, 0.02)$  while for the chaotic truth  $\epsilon = 0.5$ . Fig. 10c shows the estimates of  $q_{error}$  with time. We see that despite the parameter bias in  $\epsilon$ , the EnKF provides good estimates of the occurrences of the events in time when the model error is included, the main differences between the truth and the estimates are in the amplitudes of the signals. This can be explained as the ensemble members with model error having a wider state space in the phase diagrams and, therefore, being able to estimate the occurrences of the earthquake as the truth will be in a smaller orbit covered by the ensemble. This explains why the best estimates of the EnKF occur when the amplitudes of the estimates of the filter are higher than the values of the truth. In contrast, the less accurate estimates occur when

the filter underestimates the events' magnitude and the truth values are higher than the EnKF estimates.

These results are valuable since the correction with model error can improve the accuracy of estimating the occurrence of seismic events, even in the presence of parameter bias. Additionally, it allows simulation with a parameter that gives periodic and stable solutions with regularized formulations and still simulates and gives good estimates of aperiodic behavior. Studies in other applications, such as ocean forecasting systems, have shown the potential benefits of using model error in addressing state and parameter estimation challenges in the presence of time-varying parameters (e.g., Brasseur et al. (2005)). In their study, Brasseur et al. (2005) found that introducing model error in the estimation causes the parameters to become constant, and the model error term absorbs all variability.

#### 4. Discussion

This study explored the application of non-Gaussian data assimilation methods on the Lorenz 1996 model and the 1-D Burridge–Knoppoff model used in seismology. All methods tested yielded low RMSEs in perfect model experiments under periodic conditions for both models—the variation in results between the models links to their inherent chaotic and non-linear behaviors. We also identified and further analyzed the role of prior knowledge in updates and the impact of including a model error term for better estimates in cases of parameter bias.

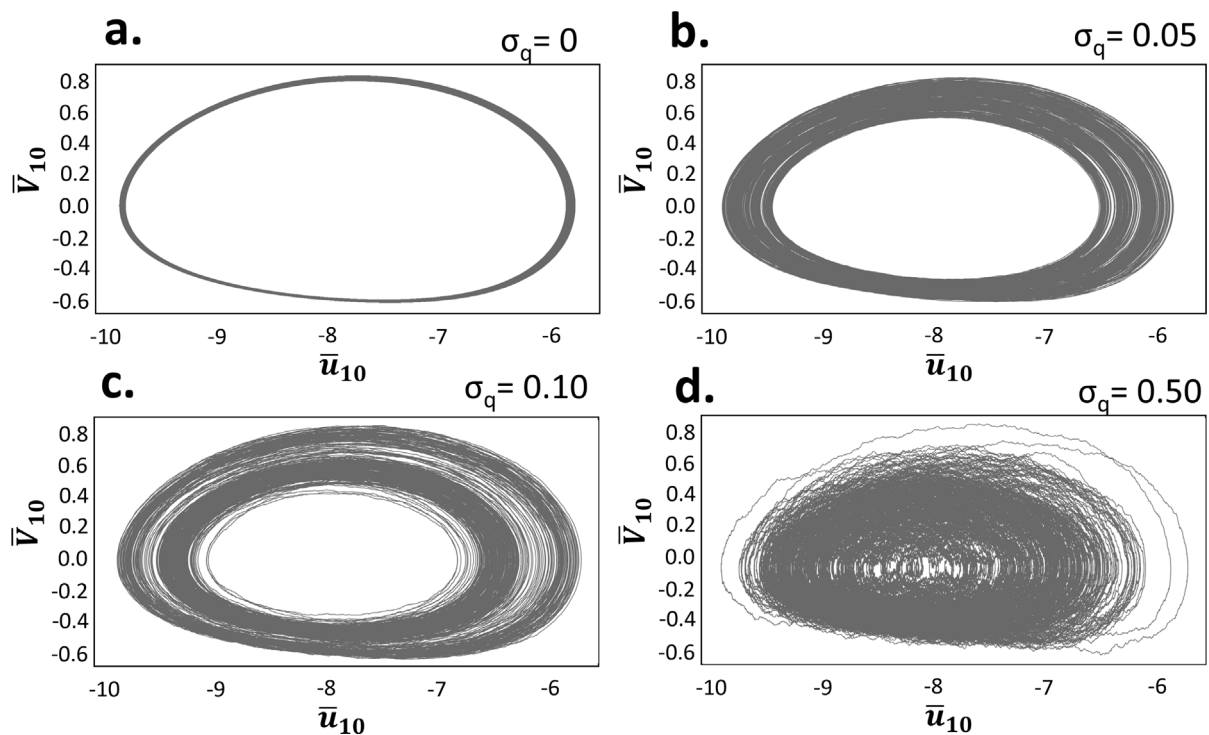


Fig. 9. Phase diagrams for different model errors: (a)  $\sigma_q = 0$ , (b)  $\sigma_q = 0.05$ , (c)  $\sigma_q = 0.1$  and (d)  $\sigma_q = 0.5$ .

#### 4.1. Comparison of the ensemble spread of the methods

In Fig. 7, we observe that the ensemble spread of the PFF is larger than that of the EnKF and the AGMF. Our analysis focused on the posterior distributions within a single assimilation step to evaluate whether the PFF's posterior spread is excessively large compared to the other methods. We used the same prior distribution and observation to evaluate this, specifically focusing on the assimilation step at time 373.5 from a perfect BK RSF 1D model experiment under periodic conditions. Prior to this step, the PFF was used for data assimilation. The prior distribution for the assimilation at  $t = 373.5$  was generated by simulating the model forward from the last assimilation step at  $t = (373)$ . We analyzed the ensemble with a histogram and used 10,000 samples, and the corresponding observation, in a particle filter to estimate a theoretical posterior distribution. As illustrated in Fig. 11, the posterior distribution derived from the PFF is not excessively broad. Instead, it is comparable to the particle filter distribution. Conversely, the EnKF shows a narrower distribution. The AGMF's estimate of the posterior distribution shows similarity to that of the particle filter and PFF at narrower values of  $h$ , but at larger  $h$  values, it exhibits a narrower distribution that is comparable to the posterior distribution of the EnKF. Fig. 7 exhibits that the posterior distributions of the EnKF tend to narrow over time when estimating the BK-RSF 1D system. All methods' distributions include the true state, as desired.

#### 4.2. PFF's sensitivity to hyperparameters and prior knowledge

In this section, we compare our findings with those of Stordal et al. (2021) who tested the Particle Flow Filter (PFF) on small chaotic systems, including the Lorenz 96 model. Their results showed that the EnKF outperforms the PFF for intermediate ensemble sizes and the Particle Filter for large ensemble sizes. Our results align with their findings for an ensemble size of 100 members, where we observed that the EnKF and PFF have very similar RMSE values. However, the advantage of our study lies in using the 1-D Burridge Knopoff model,

which is not driven by noise, unlike the setup in Stordal et al. (2021). Fig. 12 compares the results for the shear stress  $\bar{\tau}$ , slip velocity  $\bar{v}$  and the state  $\bar{\theta}$  for two configurations of the PFF. The results presented with a dashed line correspond to a PFF whose attractive term (Eq. (26)) only includes information from the likelihood, while the continuous line results include information from both the prior and the likelihood. Since the results are almost indistinguishable, it may lead to the conclusion that the filter becomes data-driven. This behavior indicates the need for further investigation to optimize the filter's performance in such cases.

#### 4.3. Limitations of the seismology model

In this study, we employed 1D seismological models, which only simulate the seismogenic zone and neglect the surrounding medium. The lower computational cost of 0D and 1D models is beneficial for understanding the effects of the rate-and-state friction law on data assimilation. However, more complex and advanced 2D and 3D models are estimated better for the evolution of stress of the seismogenic zone and in the surrounding medium (Li et al., 2022). The 3D models are especially pertinent in determining shear stress distributions at faults and the nucleation process.

We simplified our state estimation by having fixed parameters. However, as highlighted by Banerjee et al. (2023) and Hirahara and Nishikiori (2019), having biased friction parameters affects the accuracy of the velocity and shear stress estimates. Addressing these discrepancies is essential, possibly through combined state and parameter estimation or model error assessment. It is important to highlight that parameter estimation, while beneficial, can also inflate computational demands by requiring smaller time steps to maintain stability in the simulations and challenge model consistency.

#### 4.4. Implications for seismology forecasting

Dynamic source inversion, primarily used for past earthquake inversion, is now complemented by data assimilation to analyze past and

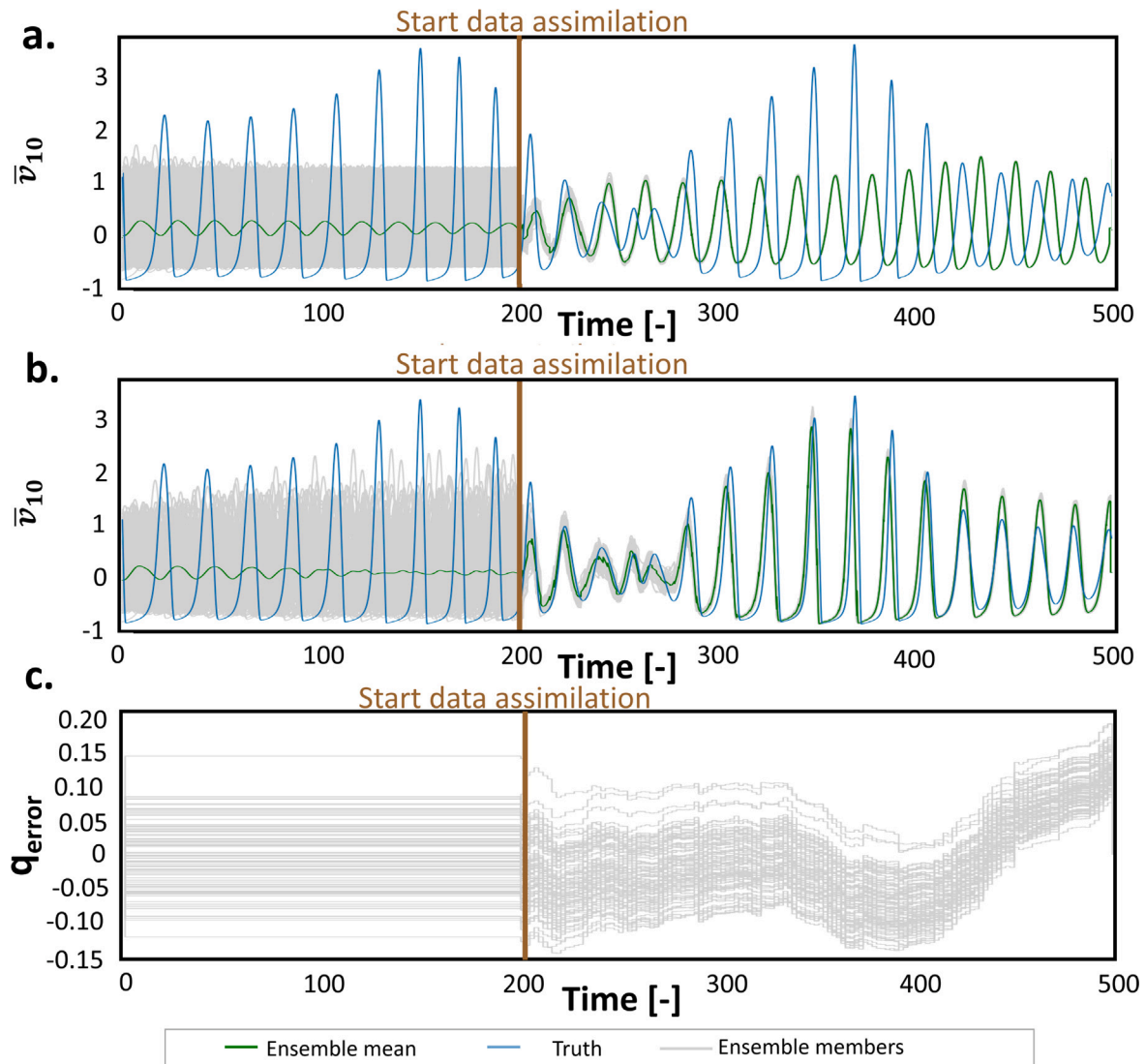


Fig. 10. Comparison of the estimates of the slip-rate  $\bar{v}$  at the block 10 of an EnKF (a) without model error and (b) with model error as part of the state vector. The mean values are in green. The truth, in blue, corresponds to the slip-rate of the chaotic model with  $\epsilon = 0.5$ . The individual ensemble members in gray are periodic with  $\epsilon = 0.3$  and model error. The synthetic observations are extracted from the chaotic synthetic truth. The results show that despite the parameter bias the EnKF estimates are in sync with the truth when including the model error especially in the occurrences of the seismic events, but with differences in the magnitude (amplitude of the signal). (c) Time series estimation of the  $q_{error}$ .

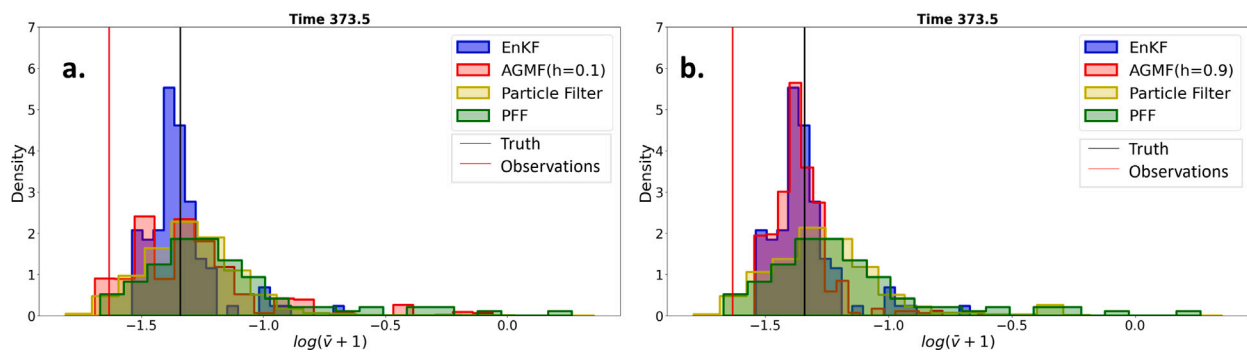


Fig. 11. Comparison of the posterior distributions of the EnKF, AGMF, PFF and a particle filter for the same assimilation step.

potential future earthquakes. Within the scope of our models and data, our research suggests that ensemble data assimilation can effectively estimate the evolution of shear stresses, velocities and state  $\theta$  in systems governed by rate-and-state friction laws, including those with chaotic behavior, aperiodicity, and varied recurrence intervals. These results

demonstrate the potential of ensemble-based approaches to provide insights into the dynamics of frictional systems with complex temporal patterns. Regularized versions of rate-and-state friction, usually yielding periodic solutions, face criticism due to origins in small-scale lab experiments. However, recent findings affirm the validity of these

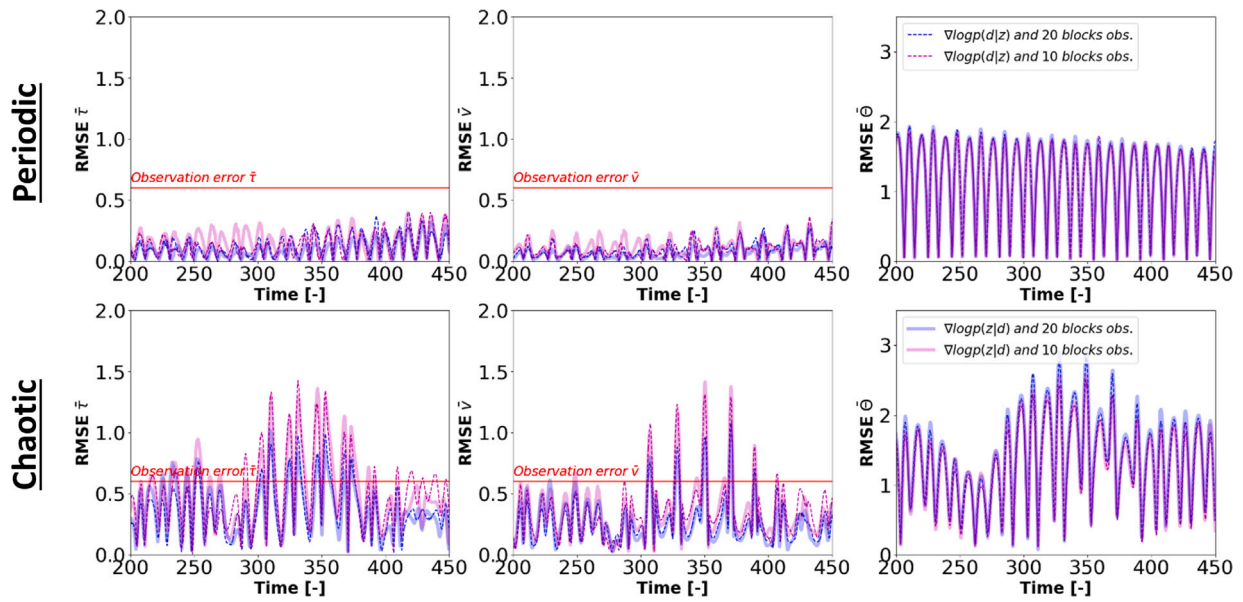


Fig. 12. Effect of the prior information in the gradient of the log posterior.

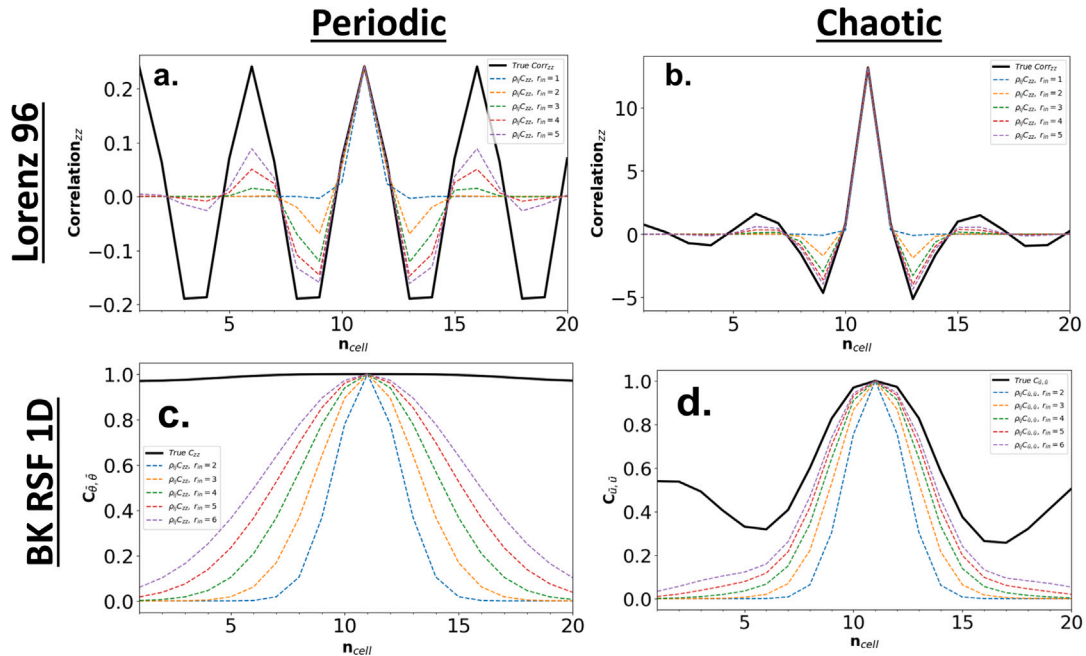


Fig. 13. Estimation of the correlation length. For the Lorenz 96 model: (a) periodic case and (b) chaotic case, with an estimated correlation length  $r_{in}$  of approximately 3. For the 1-D Burridge–Knopoff model: (c) periodic case and (d) chaotic case, with an estimated correlation length  $r_{in}$  of approximately 5.

small-scale observations for larger setups, up to a meter (Ji et al., 2022). Avoiding underdispersion when using periodic simulations in ensemble data assimilation and addressing model errors as proposed in this study is crucial for better estimates, especially in real-world scenarios.

### 5. Conclusions

In this study, we have conducted a detailed examination of the performance of the Ensemble Kalman, Adaptive Gaussian Mixture, and Particle Flow Filters applied to the Lorenz 1996 model and 1-D Burridge–Knopoff models under periodic and chaotic regimes. The Ensemble Kalman and Adaptive Gaussian Mixture Filters faced underdispersion issues, necessitating a large inflation of their prior covariance matrices. Under periodic conditions, meaning periodic seismic

cycles, the Ensemble Kalman Filter achieved the lowest RMSE, yet underdispersion remained a problem for both it and the Adaptive Gaussian Mixture Filter.

Notably, particle flow filters proved more robust against underdispersion, particularly with integrating regularized frictional laws that lead to quasi-periodic behavior. Additionally, they offered more precise estimates for unobserved variables such as the state variable  $\bar{\theta}$  in the Burridge–Knopoff models. This advantage is valuable given the scarcity of historical seismological data relative to the low frequency of significant tectonic earthquakes. Nevertheless, it is important to consider that the tuning of the bandwidth in particle flow filters can have a substantial impact on their performance. For example, certain very wide bandwidth may affect sample separation, influencing the kernel’s behavior. Hence, it is advisable to adjust the bandwidth

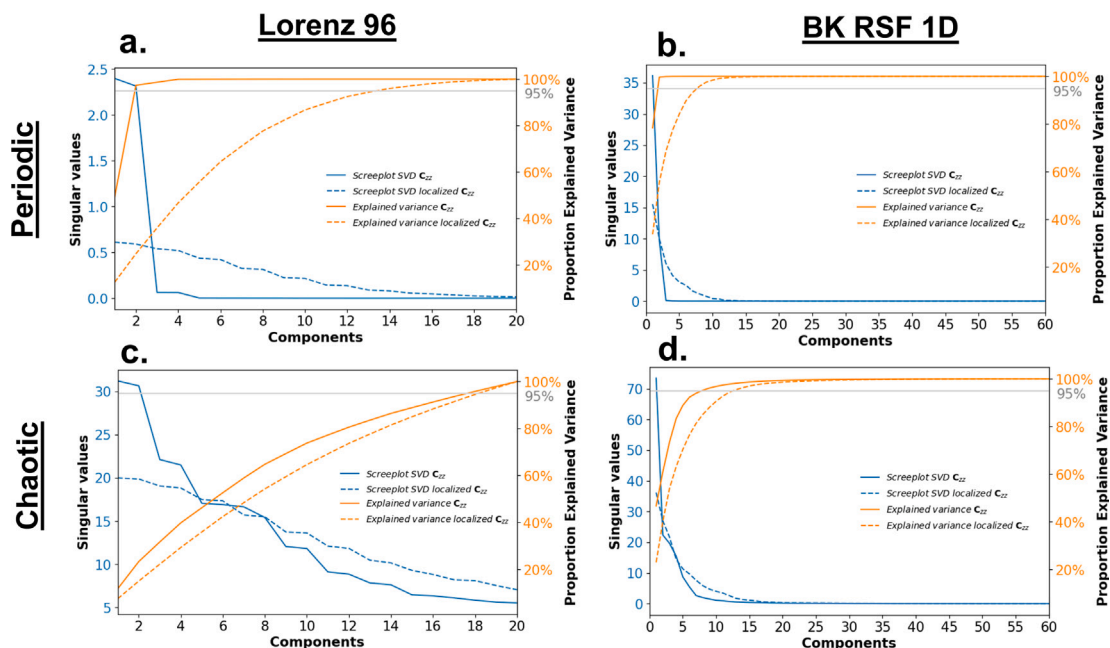


Fig. 14. Scree plot of the singular value decomposition of the prior covariance matrices ( $C_{zz}$ ) before and after localization for the Lorenz 96 (a, c) and Burridge–Knopoff model (b, d). The solid lines correspond to the decomposition of the matrices before localization, while the dashed lines to the decomposition of the matrices after the localization. The blue lines represent the distribution of singular values while the orange lines show the proportion of cumulative variance explained until that component.

hyperparameter thoughtfully.

Our results highlight the potential of ensemble data assimilation techniques to reliably estimate the evolution of shear stresses, velocities, and the state variable  $\bar{\theta}$  in earthquake models governed by chaotic dynamics and irregular recurrence intervals. Regularized versions of rate-and-state friction laws, have been scrutinized for being derived from small-scale laboratory experiments. However, recent evidence supports the relevance of these laboratory observations to larger-scale scenarios (Ji et al., 2022). Since these periodic simulations are used to explain also large-scale experiments, it is important to consider model errors and underdispersion within ensemble data assimilation frameworks.

We have also highlighted the challenges the rate-and-state friction law poses, which can cause abrupt system behavior changes due to uncertainties in frictional parameters. These uncertainties can lead to convergence issues, ensemble degeneracy, and complications in data assimilation when parameters are incorporated into the state vector of a high-dimensional system. We proposed incorporating stochastic model error terms into data assimilation as a solution, providing the necessary flexibility to accommodate a range of stable solutions and enabling the estimation of aperiodic behaviors amid predominantly periodic solutions. This approach introduces additional stochasticity in the behavior to capture earthquake dynamics more accurately with data assimilation.

Finally, we discussed how the selection of numerical models and rate-and-state friction laws can predispose systems to quasi-periodic behaviors, potentially causing underdispersion problems that compromise the reliability of estimations from methods that assume Gaussianity and linearity. We demonstrated that the Particle Flow Filter can maintain adequate variance in its estimates, which is crucial for applying laboratory or field data where the accuracy of the estimates in relation to the true state is often challenging to determine.

#### CRediT authorship contribution statement

**Hamed Ali Diab-Montero:** Writing – review & editing, Writing – original draft, Visualization, Validation, Software, Methodology, Investigation, Formal analysis, Data curation, Conceptualization. **Andreas S.**

**Stordal:** Writing – review & editing, Validation, Supervision, Methodology, Formal analysis. **Peter Jan van Leeuwen:** Writing – review & editing, Validation, Supervision, Methodology, Formal analysis. **Femke C. Vossepoel:** Writing – review & editing, Writing – original draft, Visualization, Validation, Resources, Project administration, Methodology, Investigation, Funding acquisition, Formal analysis.

#### Declaration of competing interest

The authors declare the following financial interests/personal relationships which may be considered as potential competing interests: Femke C. Vossepoel reports financial support was provided by Dutch Research Council. If there are other authors, they declare that they have no known competing financial interests or personal relationships that could have appeared to influence the work reported in this paper.

#### Acknowledgments

This publication is part of the “InFocus: An Integrated Approach to Estimating Fault Slip Occurrence” project (grant number: DEEP.NL.2018.037) funded by NWO’s (Dutch Research Council) DeepNL programme. The programme aims to improve the fundamental understanding of the dynamics of the deep subsurface under the influence of human interventions. Additionally, the authors thank Chih-Chi Hu for his help with the initial implementation of the Particle Flow Filter.

#### Code availability

Non-gaussian-data-assim library.

Contact: [ha.diabmontero@gmail.com](mailto:ha.diabmontero@gmail.com)

Program language: Python

Software required: Python

The source codes are available for downloading at the link: [https://github.com/hamed-diab-montero/non\\_gaussian\\_data\\_assim/](https://github.com/hamed-diab-montero/non_gaussian_data_assim/).

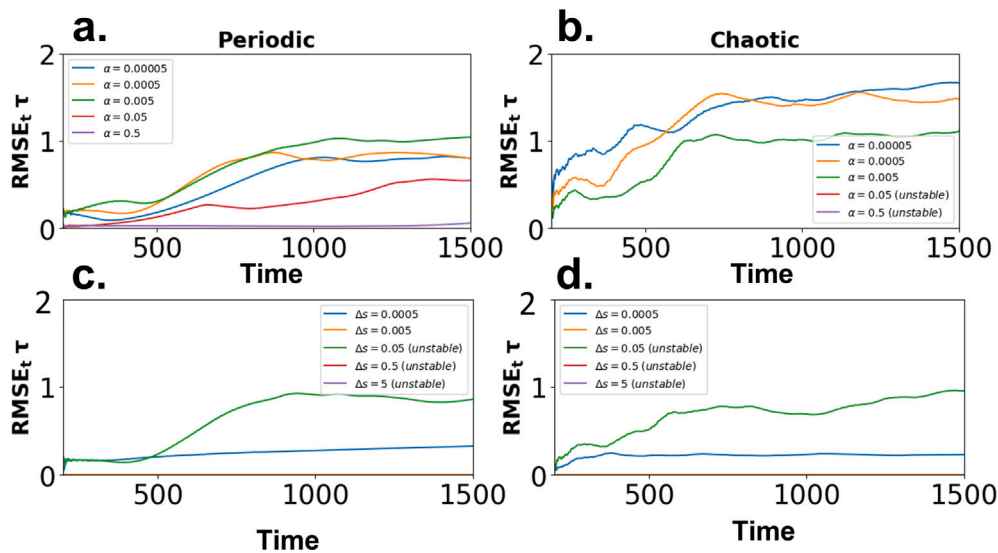


Fig. 15. Sensitivity analysis of the hyperparameter bandwidth of the kernel ( $\alpha$ ) for the Particle Flow Filter used on the BK-RSF 1D model. The left column shows the results for the periodic conditions of the BK-RSF 1D, while the right column shows the results for the chaotic condition.

## Appendix A. Analysis of the background covariances, localization and inflation

In ensemble data assimilation, methods like the Ensemble Kalman Filter rely on techniques such as localization and covariance inflation to address the limitations of small ensemble sizes and low-rank covariance matrices. A limited ensemble size can introduce long-distance correlations and underestimate forecast errors, diminishing the assimilation's accuracy. Localization counters these non-physical correlations, ensuring observations have a localized and consistent impact. Covariance inflation adjusts underestimated forecast errors, ensuring the model forecast is not underrepresented and preventing filter divergence. In this study, we use localization via a Schur product. For the Burridge–Knopoff model, we apply the Schur product carefully in each sector of the covariance matrix to conserve the cross-covariance elements between observed and unobserved variables. We used a correlation length  $r_{in}$  of 3 for the Lorenz 96 model and 5 for the 1-D Burridge–Knopoff model (Fig. 13).

We use singular value decomposition (SVD) to analyze the prior covariance matrices of the Lorenz 96 and BK models, evaluating the impact of localization on their effective rank, as shown in Fig. 14. For the Lorenz 96 model, before localization, the effective rank is 2 for the periodic case and 18 for the chaotic. After localization, the periodic case rises to 14, while the chaotic remains at 18. For the 1-D Burridge–Knopoff models coupled with rate-and-state friction, the ranks are initially 3 for the periodic and 6 for the chaotic cases. Upon localization, these numbers increase to 8 and 15, respectively.

### A.1. Inflation of covariance matrices

Our study compared the variances in state variable estimates across different ensemble sizes (10, 20, 50, 100, 200, and 500) in the context of the 1-D Burridge–Knopoff model with rate-and-state friction. The consistent variances observed suggest that using a low-rank approximation does not significantly underrepresent covariances. Hence, an inflation factor is not necessary. However, as Section 3 indicates, underdispersion was observed in periodic cases. To address this, we applied an inflation factor of 1.1, which slightly alleviated the underdispersion while maintaining simulation stability. Larger inflation factors were found to cause instability post-assimilation steps.

## Appendix B. Selection of hyperparameters

### B.1. Hyperparameter selection for the adaptive Gaussian mixture filter and the particle flow filter

For the AGMF, we tested different bandwidths for the Gaussian mixtures, denoted as  $h$ . We used a default value of 0.6. An analysis of the RMSE, STD, and the rank histogram showed a lower error for lower  $h$  values (around 0.2) in the periodic case of the Lorenz 96 and values closer to 0.6 in the chaotic case. Such low values of  $h$  are inconsistent with the high inflation factors needed to avoid underdispersion. For this reason, we adhered to a value of 0.6. This approach was also applied to the Burridge–Knopoff models.

The particle flow filter has two hyperparameters: the kernel bandwidth ( $\alpha$ ) and the pseudo-time step size ( $\Delta s$ ). We tested 5 bandwidths (0.00005, 0.0005, 0.005 and 0.5) and 5 pseudo-time steps (0.0005, 0.005, 0.05, 0.5 and 5). The selected bandwidths from Fig. 15 were 0.05 for periodic and 0.0005 for chaotic conditions of the BK RSF 1D model. For periodic conditions, a bandwidth of 0.05 yielded the lowest RMSE without filter collapse. For chaotic conditions, a bandwidth of 0.0005 ensured stable results. A pseudo-time step of 0.0005 was chosen for both conditions, minimizing RMSE while avoiding filter collapse.

### Data availability

The data produced and analyzed in this study is available via 4TU.ResearchData <http://doi.org/10.4121/f0f075f2-f45c-4f8c-9d1d-bde03baeae33>.

### References

- Aanonsen, S.I., Naevdal, G., Oliver, D.S., C., R.A., Valles, B., 2009. Ensemble Kalman filter in reservoir engineering—A review. *SPE J.* 14, 393–412. <http://dx.doi.org/10.21188/117274-PA>.
- Anderson, J.L., 1996. A method for producing and evaluating probabilistic forecasts from ensemble model integrations. *J. Clim.* 9 (7), 1518–1530.
- Banerjee, A., van Dinther, Y., Vossepoel, F.C., 2023. On parameter bias in earthquake sequence models using data assimilation. *Nonlinear Process. Geophys.* 30 (2), 101–115. <http://dx.doi.org/10.5194/npg-30-101-2023>, URL: <https://npg.copernicus.org/articles/30/101/2023/>.

- Bannister, R.N., 2017. Review article: A review of operational methods of variational and ensemble-variational data assimilation. *Q. J. R. Meteorol. Soc.* 143, 607–633. <http://dx.doi.org/10.1002/qj.2982>.
- Brasseur, P., Baharel, P., Bertino, L., Birol, F., Brankart, J.-M., Ferry, N., Losa, S., Rémy, E., Schröter, J., Skachko, S., et al., 2005. Data assimilation for marine monitoring and prediction: The mercator operational assimilation systems and the MERSEA developments. *Q. J. R. Meteorol. Soc.* A 131 (613), 3561–3582.
- Burridge, R., Knopoff, L., 1967. Model and theoretical seismicity. *Bull. Seismol. Soc. Am.* (ISSN: 0037-1106) 57 (3), 341–371. <http://dx.doi.org/10.1785/BSSA0570030341>.
- Carlson, J.M., Langer, J.S., Shaw, B.E., Tang, C., 1991. Intrinsic properties of a Burridge–Knopoff model of an earthquake fault. *Phys. Rev. A* 44 (2), 884.
- Carrasi, A., Bocquet, M., Demaeyer, J., Grudzien, C., Raanes, P., Vannitsem, S., 2022. Data assimilation for chaotic dynamics. In: *Data Assimilation for Atmospheric, Oceanic and Hydrologic Applications*, Vol. IV. Springer, pp. 1–42.
- Crupi, P., Bizzarri, A., 2013. The role of radiation damping in the modeling of repeated earthquake events. *Ann. Geophys.*
- Diab-Montero, H.A., Li, M., van Dinther, Y., Vossepoel, F.C., 2023. Estimating the occurrence of slow slip events and earthquakes with an ensemble Kalman filter. *Geophys. J. Int.* 234 (3), 1701–1721.
- Dieterich, J.H., 1979. Modeling of rock friction: 1. Experimental results and constitutive equations. *J. Geophys. Res.* 84, <http://dx.doi.org/10.1029/JB084iB05p02161>.
- Erickson, B., Birnir, B., Lavallée, D., 2008. A model for aperiodicity in earthquakes. *Nonlinear Process. Geophys.* 15 (1), 1–12. <http://dx.doi.org/10.5194/npg-15-1-2008>.
- Erickson, B.A., Birnir, B., Lavallée, D., 2011. Periodicity, chaos and localization in a Burridge–Knopoff model of an earthquake with rate-and-state friction. *Geophys. J. Int.* 187 (1), 178–198. <http://dx.doi.org/10.1111/j.1365-246X.2011.05123.x>.
- Evensen, G., 1994. Sequential data assimilation with a nonlinear quasi-geostrophic model using Monte Carlo methods to forecast error statistics. *Comput. Geosci.* 99, 10143–10162. <http://dx.doi.org/10.1029/94JC00572>.
- Evensen, G., 2003. The ensemble Kalman filter: Theoretical formulation and practical implementation. *Ocean Dyn.* 53, 343–367. <http://dx.doi.org/10.1007/s10236-003-0036-9>.
- Evensen, G., Eikrem, K.S., 2018. Strategies for conditioning reservoir models on rate data using ensemble smoothers. *Comput. Geosci.* 22, 1251–1270. <http://dx.doi.org/10.1007/s10596-018-9750-8>.
- Evensen, G., Vossepoel, F.C., van Leeuwen, P.J., 2022. *Data Assimilation Fundamentals: A Unified Formulation of the State and Parameter Estimation Problem*, first ed. Springer, ISBN: 978-3-030-96708-6, p. 254. <http://dx.doi.org/10.1007/978-3-030-96709-3>, Open access.
- Gualandi, A., Faranda, D., Marone, C., Cocco, M., Mengaldo, G., 2023. Deterministic and stochastic chaos characterize laboratory earthquakes. *Earth Planet. Sci. Lett.* 604, 117995.
- Hamill, T.M., 2001. Interpretation of rank histograms for verifying ensemble forecasts. *Mon. Weather Rev.* 129 (3), 550–560.
- Hirahara, K., Nishikiori, K., 2019. Estimation of frictional properties and slip evolution on a long-term slow slip event fault with the ensemble Kalman filter: numerical experiments. *Geophys. J. Int.* 219, 2074–2096. <http://dx.doi.org/10.1093/gji/ggz415>.
- Hori, T., Miyazaki, S., Hyodo, M., Nakata, R., Kaneda, Y., 2014. Earthquake Forecasting System Based on Sequential Data Assimilation of Slip on the Plate Boundary, vol. 62, pp. 179–189. <http://dx.doi.org/10.11345/nctam.62.179>.
- Hu, C.-C., Jan, v.P., Anderson, J.L., 2024. An implementation of the particle flow filter in an atmospheric model. *Mon. Weather Rev.* 152 (10), 2247–2264.
- Hu, C.-C., van Leeuwen, P.J., 2021. A particle flow filter for high-dimensional system applications. *Q. J. Roy. Meteor. Soc.* 147, 2352–2374. <http://dx.doi.org/10.1002/qj.4028>.
- Ji, Y., Niemeijer, A., Baden, D., Yamashita, F., Xu, S., Hunfeld, L., Pijnenburg, R.P., Fukuyama, E., Spiers, C., 2022. Friction law for earthquake nucleation: size doesn't matter.
- Kano, M., Miyazaki, S., Ito, K., Hirahara, K., 2013. An adjoint data assimilation method for optimizing frictional parameters on the afterslip area. *Earth, Planets Space* 65, 1575–1580. <http://dx.doi.org/10.1029/2019JB019047>.
- Lapusta, N., Rice, J.R., 2003. Nucleation and early seismic propagation of small and large events in a crustal earthquake model. *J. Geophys. Res. Solid Earth* 108 (B4).
- Li, M., Pranger, C., van Dinther, Y., 2022. Characteristics of earthquake cycles: A cross-dimensional comparison of OD to 3D numerical models. *J. Geophys. Res. Solid Earth* <http://dx.doi.org/10.1029/2021JB023726>, e2021JB023726.
- Liu, Y., Weerts, A.H., Clark, M., Hendricks Franssen, H.J., Kumar, S., Moradkhani, H., Seo, D.J., Schwanenberg, D., Smith, P., van Dijk, A.L.J.M., van Velzen, N., He, M., Lee, H., Noh, S.J., Rakovec, O., Restrepo, P., 2012. Advancing data assimilation in operational hydrologic forecasting: Progresses, challenges, and emerging opportunities. *Hydrol. Earth Syst. Sci.* 16, 3863–3887. <http://dx.doi.org/10.5194/hess-16-3863-2012>.
- Lorenz, E.N., Emanuel, K.A., 1998. Optimal sites for supplementary weather observations: Simulation with a small model. *J. Atmos. Sci.* 55 (3), 399–414. [http://dx.doi.org/10.1175/1520-0469\(1998\)055<0399:OSFSWO>2.0.CO;2](http://dx.doi.org/10.1175/1520-0469(1998)055<0399:OSFSWO>2.0.CO;2).
- Lu, J., Lu, Y., Nolen, J., 2019. Scaling limit of the stein variational gradient descent: The mean field regime. *SIAM J. Math. Anal.* 51 (2), 648–671.
- Madariaga, R., 1998. Study of an oscillator of single degree of freedom with dieterich-ruina rate and state friction, Laboratoire de Géologie, Ecole Normale Supérieure. pp. 643–696, Unpublished Notes.
- Maeda, T., Obara, K., Shinohara, M., Kanazawa, T., Uehiro, K., 2015. Successive estimation of a tsunami wavefield without earthquake source data: A data assimilation approach toward real-time tsunami forecasting. *Geophys. Res. Lett.* <http://dx.doi.org/10.1002/2015GL065588>.
- Marone, C., 1998. Laboratory-derived friction laws and their application to seismic faulting. *Annu. Rev. Earth Planet. Sci.* 26 (1), 643–696.
- Noda, H., Dunham, E.M., Rice, J.R., 2009. Earthquake ruptures with thermal weakening and the operation of major faults at low overall stress levels. *J. Geophys. Res. Solid Earth* 114 (B7).
- Oba, A., Furumura, T., Maeda, T., 2020. Data assimilation-based early forecasting of long-period ground motions for large earthquakes along the nankai trough. *J. Geophys. Res. Solid Earth* <http://dx.doi.org/10.1029/2019JB019047>.
- Reichle, R.H., 2008. Data assimilation methods in the Earth Sciences. *Adv. Water Resour.* 31, <http://dx.doi.org/10.1016/j.advwatres.2008.01.001>.
- Rojas, O., Dunham, E.M., Day, S.M., Dalguer, L.A., Castillo, J.E., 2009. Finite difference modelling of rupture propagation with strong velocity-weakening friction. *Geophys. J. Int.* 179 (3), 1831–1858.
- Ruina, A., 1983. Slip instability and state variable friction laws. *J. Geophys. Res.* 88.
- Stordal, A.S., Karlsen, H.A., Nævdal, G., Skaug, H.J., Vallès, B., 2011. Bridging the ensemble Kalman filter and particle filters: the adaptive Gaussian mixture filter. *Comput. Geosci.* 15, 293–305.
- Stordal, A.S., Lorentzen, R.J., 2014. An iterative version of the adaptive Gaussian mixture filter. *Comput. Geosci.* 18, 579–595.
- Stordal, A.S., Moraes, R.J., Raanes, P.N., Evensen, G., 2021. p-Kernel Stein variational gradient descent for data assimilation and history matching. *Math. Geosci.* 53 (3), 375–393.
- van Dinther, Y., Künsch, H.R., Fichtner, A., 2019. Ensemble data assimilation for earthquake sequences: probabilistic estimation and forecasting of fault stresses. *Geophys. J. Int.* 217, <http://dx.doi.org/10.1093/gji/ggz063>.
- van Kekem, D.L., 2018. Dynamics of the lorenz-96 model: Bifurcations, symmetries and waves.
- van Leeuwen, P.J., 2010. Nonlinear data assimilation in geosciences: An extremely efficient particle filter. *Q. J. R. Meteorol. Soc.* 136, 1991–1999. <http://dx.doi.org/10.1002/qj.699>.
- Van Leeuwen, P.J., Künsch, H.R., Nerger, L., Potthast, R., Reich, S., 2019. Particle filters for high-dimensional geoscience applications: A review. *Q. J. R. Meteorol. Soc.* 145 (723), 2335–2365.